Multisensory gamma stimulation enhances adult neurogenesis and improves cognitive function in a mouse model of Down syndrome

Md Rezaul Islam*[1], Brennan Jackson*[1,2], Brooke Schatz[1], Mitchell Murdock[1,3], Noah Tan[1], Dong Shin Park[1], Daniela Rodrigues Amorim[1], Fred Jiang[4], S. Sebastian Pineda[5], Chinnakkaruppan Adaikkan[1], Vanesa Fernandez[1], Ute Geigenmuller[1], Manolis Kellis[5,6], Edward S. Boyden[4,7,8], Li-Huei Tsai[1,3#]

Affiliations
[1]Picower Institute for Learning and Memory, Massachusetts Institute of Technology, Cambridge, MA, USA.
[2]Institute for Medical Engineering and Science, Massachusetts Institute of Technology, Cambridge, MA, USA.
[3]Department of Brain and Cognitive Sciences, Massachusetts Institute of Technology, Cambridge, MA, USA.
[4]Departments of Biological Engineering and Brain and Cognitive Sciences, McGovern Institute, Cambridge, MA, USA.
[5]MIT Computer Science and Artificial Intelligence Laboratory, Cambridge, MA, USA.
[6]Broad Institute of MIT and Harvard, Cambridge, MA, USA.
[7]Koch Institute, Massachusetts Institute of Technology, Cambridge, MA, USA.
[8]Howard Hughes Medical Institute, Massachusetts Institute of Technology, Cambridge, MA, USA.

*Equal contribution
#Corresponding author; Li-Huei Tsai, PhD; E-mail: lhtsai@mit.edu

Summary
Down syndrome (DS) has been linked with deficits in hippocampal dependent cognitive tasks and adult neurogenesis, yet treatment options are still very limited. We and others previously showed that a non-invasive multisensory gamma stimulation using light and sound at 40 Hz ameliorated Alzheimer's disease pathology and symptoms in mouse models. In this study, we tested the effects of 40 Hz multisensory stimulation in the Ts65Dn mice, a mouse model of DS. For three weeks, mice were exposed daily to one hour of stimulation or one hour of ambient light and sound. Mice receiving the stimulation showed improved object recognition and spatial working memory. Using single nuclei RNA-seq and experimental validations in mouse hippocampal samples, we identified underlying expression changes in gene regulatory networks and demonstrated increased adult neurogenesis and reorganization of synapses as potential mechanisms for these improved cognitive phenotypes. Together, our data reveal a novel effect of multisensory gamma stimulation on adult neurogenesis and beneficial effects of 40 Hz treatment on cognitive function in DS model mice.

Keywords: Multisensory gamma stimulation; 40 Hz; single nuclei RNA-seq; gene-regulatory network; Down syndrome; non-invasive therapy

Significance Statement
We present strong evidence, using a well-characterized mouse model, that the cognitive and neurogenesis deficits in Down syndrome can be improved through non-invasive multi-sensory gamma stimulation. Employing a systems biology approach, we provide extensive hippocampal single-cell resolution gene expression signatures and changes in gene regulatory networks in response to sensory gamma stimulation.

Main Text

Introduction

Down syndrome (DS) has been linked with impaired neurogenesis[1] and aberrant synaptic functions in the hippocampus[2]. These changes are consistent with the reported deficits in memory and other cognitive tasks in individuals with DS [3,4]. Additionally, a recent study found dementia to be associated with mortality in 70% of older adults with DS [5]. However, there are currently limited therapeutic options available to manage cognitive performance in individuals with DS. We have previously reported the utility of using sensory stimulation presented at gamma frequency for combating cognitive decline in mouse and human subjects[6–8]. The sensory gamma stimulation reduced Alzheimer's disease (AD) related pathology, improved neuronal survival and synaptic density, and enhanced cognitive function in multiple mouse models of AD[7,9,10]. Others have also reported the beneficial effects associated with gamma stimulation in AD[11–13] as well as in other neurological diseases such as Parkinson´s disease[14]. However, efficacy of sensory gamma stimulation has not been tested in DS. Here, we used a well-characterized DS mouse model, Ts65Dn mice, to test the effects of sensory gamma stimulation and observed that this treatment improved cognitive function, enhanced adult neurogenesis, and induced expression changes in genes involved in synaptic organization.

Results

Multisensory gamma stimulation improves cognitive performance of Ts65Dn mice

To examine the effect of the sensory gamma stimulation on cognitive performance in DS, we used the Ts65Dn mouse model of DS, which recapitulates phenotypes present in individuals with DS including synaptic abnormalities[15] and deficits in hippocampal-dependent spatial learning and memory[16] and adult neurogenesis[17]. We exposed one group of Ts65Dn mice to one hour of 40 Hz auditory and visual stimulation per day (stimulation), while a parallel group was exposed to ambient light and sound (ambient, **Fig 1A**). Littermate wild-type controls were not included in this experimental setup since the well-established cognitive deficits of Ts65Dn mice in hippocampus-dependent tasks, as reported in previous studies [18–20], offer a clear benchmark for evaluating the effects of stimulation on cognitive improvements. Shortly before the completion of the three-week treatment period using the 40 Hz or ambient auditory and visual stimulation, we conducted the Novel Object Recognition (NOR), Novel Object Location (NOL), and elevated Y-maze behavioral tests to evaluate the effects of the stimulation on object recognition (**Fig 1B**) and spatial memory (**Fig 1C-D**). For the NOR/NOL tests, both groups of mice were first presented with two objects in fixed locations. When one of the familiar objects was later replaced by a novel object in the same location (NOR, **Fig 1B**) or placed in a novel location (NOL, **Fig 1C**), the stimulation group spent a significantly higher percentage of time than the ambient group exploring the novel object (stimulation = 64.1+/-12.3%, ambient = 48.6+/-21.5%, $p = 0.04$) and the familiar object in the

novel location (stimulation = 73.4+/-11.7% vs ambient = 46.6+/-15.4%, $p < 0.001$). Importantly, the observed changes in performance between stimulation and ambient groups were not related to differences in locomotory behaviors in an open field area (**Fig S1A, Fig S1B**). Thus, the NOR/NOL results indicate a clear improvement in both object recognition and spatial memory in the stimulation group compared to the ambient group. Spatial memory was further assessed by spontaneous alternation in the elevated Y-maze test, which allows mice to freely explore the three arms of a Y-shaped maze. Consecutive entries into three different arms are considered a spontaneous alternation, expressed as % of all possible entry triads. Mice with stimulation demonstrated a significantly higher number of spontaneous alternations than the ambient group (stimulation = 61.15+/-9.1%, ambient = 51.3+/-8.7%, $p = 0.02$, **Fig 1D**), while the number of total entries was not significantly different between the two groups (stimulation = 29.2+/-7.9, ambient = 24.1+/-6.3, **Fig 1D**). These results indicate improved spatial working memory in DS mice in response to stimulation. Since both object recognition and spatial memory are hippocampus-dependent memory tasks, the behavioral testing results also imply that the sensory stimulation impacts hippocampal neurons. This was experimentally confirmed by performing staining for c-Fos, a widely used marker of neuronal activity [21], on brain sections from mice in the stimulation and ambient groups. Mice in the stimulation group showed increased number of c-Fos positive nuclei in the hippocampus compared to mice in the ambient group (**Fig S2**).

Multisensory gamma stimulation increases expression of synapse-related genes in excitatory neurons in the hippocampus of Ts65Dn mice

To decipher potential mechanisms underlying sensory stimulation-mediated cognitive improvement in Ts65Dn mice, we performed single-nucleus RNA sequencing (snRNA-seq) on hippocampal samples from the stimulated and ambient groups of mice (**Fig 2A)**, yielding 15,884 nuclei with high quality transcriptomic profiles (**Fig S3**). Based on the top variable genes, the nuclei were categorized into transcriptionally distinct clusters that could be visualized in uniform manifold approximation and projection (UMAP) space and assigned to principal brain cell types based on the expression of canonical markers (**Fig 2B, Fig S3E**). The majority (69.7%) of captured nuclei represented neurons (54.5% excitatory and 15.2% inhibitory), 26.5% were derived from glial cells, and the remaining 3.8% represented vascular and choroid plexus cells (**Fig S3F**). Samples were well integrated across both groups (**Fig S3G**), and broad cell type constituency did not differ significantly between the stimulation and ambient groups (**Fig S3H)**.

We then performed differential gene expression analyses focusing on the neuronal clusters. Excitatory neurons showed a higher number of gene expression changes in response to the stimulation than inhibitory neurons, with 108 genes upregulated and 104 genes downregulated in the stimulation group compared to the ambient group (**Fig 2C**, **Table S1**). Using a curated list of synaptic genes as reference [22], we found that synaptic genes were significantly overrepresented within the set of 108 upregulated genes (overrepresentation test, p value = 0.004; **Table S2**).

125 Differentially upregulated synaptic genes included *Actb, Actg1, Atp6voc, Camk2b, Frrs1l, Gphn,*
126 *Gpm6a, Hspa8, Il1rapl1, Mdga2, Nptn, Nrg1, Rab14, Rock1, Syt11*, and *Tuba1a*, of which several
127 have been implicated in synaptic functions [23], synapse development [24], or synaptic plasticity [25].
128 Gene ontology (GO) analyses further demonstrated that the genes differentially expressed in
129 excitatory neurons in response to stimulation were associated with various synaptic functions, with
130 the majority related to synapse organization (e.g., synaptic vesicle endocytosis, synapse assembly,
131 synapse organization, post-synapse organization, regulation of synapse organization, and
132 regulation of synapse structure) (**Fig 2D**), and that some of these processes were also altered in
133 inhibitory neurons (**Fig 2D**). Of note, reanalysis of published datasets (see Methods) unveiled
134 downregulation of synapse organization associated genes in the brains of Ts65Dn mice (**Fig S4A-**
135 **B, Table S3**) as well as in excitatory neurons in individuals with DS (**Fig S4C, Table S3**)
136 compared to healthy controls.
137
138 To strengthen these findings in excitatory neurons and for additional insights, we employed an
139 orthogonal computational approach. Using a weighted gene co-expression analysis (WGCNA), we
140 identified seven gene regulatory modules in hippocampal excitatory neurons (**Fig 2E, Table S4,**
141 **Fig S5A-B**). Three of these seven gene modules (Ex-3, Ex-6, Ex-7) showed significantly increased
142 expression in the stimulation group compared to the ambient group, two (Ex-1 and Ex-2) displayed
143 decreased expression (**Fig 2E**, **Fig S5C**), and two (Ex-4, Ex-5) showed no expression changes (**Fig**
144 **2E**). Focusing our downstream analyses on the three upregulated gene modules, we found that
145 several of the hub genes encode synaptic proteins (**Fig 2F**) and few of these genes are implicated
146 in synaptic organization (Farp1[30]), synapse formation (Ptprt[31]) and synapse development (Lrrc4c[32],
147 Efna5[33]). Therefore, increased expression of these three gene modules may alter functional
148 synapses in the hippocampus of the stimulation group.

149 To test this hypothesis experimentally, we performed immunostaining for the post-synaptic marker
150 PSD95 and the pre-synaptic marker synaptophysin in the granule cell molecular layer of the
151 dentate gyrus in the hippocampi from the ambient and stimulation groups (**Fig 2H**). Co-
152 localization of both markers served as the readout of functional/mature synapses. The stimulation
153 group showed a significant increase in the number of mature synapses in the dentate gyrus (**Fig**
154 **2H**). These findings confirm that the gene expression changes observed in response to stimulation
155 lead to modification in synaptic organization within the hippocampus.

156 Further analyses unveiled several hub genes that are associated with Alzheimer´s Disease (AD)
157 related dementia (**Fig 2I)**. Among those, *Reln* in particular has been implicated in AD[34,35] and
158 aging[36], and a gain-of-function variant in this gene has been shown to confer resilience against
159 autosomal dominant AD [37]. Remarkably, IHC unveiled an increased proportion of *Reln*+ neurons
160 in the hippocampus of our stimulation group compared to the ambient group (**Fig 2J**).
161

Based on these observations and to further validate the significance of the three gene modules in cognitive benefits, we examined their expression patterns in published transcriptomic datasets (see Methods) focusing on aging and AD, both known risk factors for cognitive decline. Interestingly, we observed reverse expression pattern of these gene modules in context to the cognitive decline. Specifically, all three modules showed a steady decrease in expression with increasing age (**Fig S6**). In line with this, the gene modules particularly module Ex-3 and Ex-7 (both increased after stimulation), significantly overlapped with genes downregulated in excitatory neurons with aging (**Fig 2K, Table S5**) or AD (**Fig 2L, Table S6**) in mice and humans. Together, these data further confirm that gamma stimulation can increase expression of cognitively relevant gene modules in excitatory neurons and thus potentially contribute to the observed cognitive benefits.

Multisensory gamma stimulation increases adult neurogenesis in Ts65Dn mice

Since the Ex-7 (61 genes) module most consistently displayed overlap across aging and AD datasets in both mouse and humans (Fig 2K, 2L), we analyzed the transcription factors (TFs) for this module to identify upstream regulators. Among the TFs whose targets overlap with the module genes, TCF4 emerged as the highest ranked transcription factor when using a p value based on a hypergeometric test (**Fig 3A**, **Table S7**). TCF4 is a critical regulator that facilitates adult neurogenesis[38], and we observed increased TCF4 expression in the dentate gyrus of Ts65Dn mice after gamma stimulation(**Fig 3B**). Thus, we hypothesized that the stimulation might have an impact on adult neurogenesis.

Previous studies have leveraged snRNA-seq datasets, specifically the transcriptional profile of granule cells (GCs), to address adult neurogenesis in mice [39] and in humans [40]. To investigate whether gamma stimulation can affect adult neurogenesis, we sorted nuclei based on the expression of Prox1, a pan-GC marker [39,41], and selected GC using an *in silico* approach (Materials and Methods). We ordered cells along the GC developmental trajectory, identified genes whose expression changed as a function of pseudotime (**Fig S7A**), and then analyzed the effect of gamma stimulation on gene expression changes along this GC developmental trajectory (**Table S8**). GO analysis revealed that 40 Hz stimulation induced differential expression of genes related to biological processes of various themes related to adult neurogenesis (e.g., neuron projection development, synapse organization, regulation of RNA splicing, microtubule-based transport, and cell morphogenesis involved in neuron differentiation) (**Fig S7B**) and that some of these processes overlapped with those reported to be downregulated in immature GCs in aging[40] .When specifically analyzing immature GCs in this study, we found three subclusters (**Fig 3C**) that expressed specific marker genes (**Fig 3D**). Among these clusters, cluster 3 was transcriptionally distinct from the other two clusters (**Table S9**), with its differentially expressed genes associated with adult neurogenesis-related biological processes (e.g., neuron migration, regulation of neurogenesis, oxidative phosphorylation, and cellular respiration) (**FigS7C-D)**. Intriguingly, the proportion of cluster 3 was significantly increased in the stimulation group (**Fig 3E-F)** compared to ambient group**,** suggesting increased neurogenesis.

202 To experimentally validate the impact of gamma stimulation on adult neurogenesis, we adopted
203 two different experimental approaches for directly testing for cell proliferation in the dentate gyrus.
204 In the first approach, fixed brain slices from both the stimulation and ambient groups were stained
205 for Ki67, a marker for cellular proliferation (**Fig 3G**). The stimulation group exhibited a
206 significantly higher number of Ki67+ cells in the sub-granular zone of the dentate gyrus compared
207 to ambient group (stimulation = 18.3+/-1.3, ambient = 12.0+/-4.4, p = 0.027, **Fig 3G**), suggesting
208 increased neurogenesis. In the second approach, a separate cohort of stimulation and ambient
209 Ts65Dn mice were injected with EdU (25 mg/kg), a nucleoside analog of thymidine that labels
210 newly synthesized DNA and thus proliferating cells, for 2 days prior to perfusion (**Fig 3H)**. In this
211 cohort, mice in the stimulation group showed a significant increase in the number of cells positive
212 for EdU in the dentate gyrus (stimulation = 8.1+/-3.1, ambient = 4.5+/-2.9, p = 0.03, **Fig 3H**),
213 again indicating that 40 Hz sensory stimulation increased adult neurogenesis in TsD65n mice.

214 Together, our results demonstrate that 40Hz stimulation can increase adult neurogenesis and
215 improve cognitive performance in the Ts65Dn mouse model. Furthermore, our findings suggest
216 that these improvements are related to changes in the expression of hippocampal gene regulatory
217 networks that are involved in synaptic organization within the hippocampus and show association
218 with aging and AD and to enhanced adult neurogenesis.

219

220 Discussion

221 In this study, we investigated the efficacy of a non-invasive multisensory gamma stimulation to
222 improve cognitive functions in Ts65Dn mice, a widely used mouse model of DS. Our study reveals
223 beneficial effects of sensory gamma stimulation on cognitive performance in hippocampal-
224 dependent tasks and on adult neurogenesis and provides hippocampal gene expression signatures
225 and gene regulatory networks at the single cell resolution. We show that three weeks of daily one-
226 hour multisensory stimulation improved spatial memory and object recognition in Ts65Dn mice.
227 Importantly, these changes were not confounded by locomotory behaviors, suggesting gamma
228 stimulation-specific effects on hippocampal-dependent memory and recognition, which is
229 consistent with previous observations in mouse models of AD and neurodegeneration [6,7].
230

231 The specific impact of the sensory gamma stimulation on transcriptomic changes and gene
232 regulatory network within the hippocampus, particularly at the single cell level, has not previously
233 been investigated. Here, we used snRNA-seq of hippocampal tissue from Ts65Dn mice to describe
234 the hippocampal molecular signatures underlying the spatial cognitive benefits from sensory
235 gamma stimulation. We showed that the stimulation increased expression of genes related to
236 synapse organization in excitatory neurons. Moreover, we identified specific gene regulatory
237 modules upregulated by 40 Hz stimulation within the excitatory neurons that significantly overlap
238 with genes downregulated during aging and in AD. This finding further highlights the relevance
239 of these gene modules for cognitive benefits. Sensory-evoked modulation of these genes are
240 particularly intriguing given that early clinical studies have shown sensory 40 Hz stimulation –

which is non-invasive, inexpensive, and easily administered in a home setting – to be safe and tolerable in humans [11]. Several of the hub genes in the gene modules with increased expression after the sensory treatment have been implicated in learning and memory, general cognitive function, and/or AD based on GWAS studies, such as *Adcy8*, *Gria4* or *Reln*. A potential role of Reelin in providing cognitive benefits in DS mice is further supported by experimental confirmation of a relative increase in *Reln*+ neurons after 40 Hz stimulation.

We further identified *TCF4*, a critical factor that facilitates adult neurogenesis[38], as one of the upstream regulators for the most conserved gene module and not only observed a notable increase in *TCF4* expression in the dentate gyrus after 40Hz stimulation, but directly demonstrated an increase in adult neurogenesis in the dentate gyrus of Ts65Dn mice. Although the exact role of adult hippocampal neurogenesis on memory continues to be elucidated, extensive evidence has shown its connection to hippocampus dependent tasks both under conditions that deplete neurogenesis [42] as well as conditions that promote neurogenesis (e.g., genetic[43] or pharmacological [44] interventions, exercise [45], and environmental enrichment [46]). In Ts65Dn mice, specifically, interventions that rescue neurogenesis have been shown to lead to improvements in novel object recognition and novel object location [47–50].

Additionally, we noted that 40 Hz stimulation increased expression of genes related to synaptic organization and the number of functional synapses, as identified by co-localization of PSD95 puncta with pre-synaptic synaptophysin puncta, in the dentate gyrus. It is likely that these hippocampal synaptic changes along with increased neurogenesis underlie the improved hippocampal-dependent tasks in 40Hz stimulation.

The present study reveals a beneficial impact of three-week long 40 Hz multisensory gamma stimulation of adult Ts65Dn male mice on their cognitive performance, neurogenesis, and hippocampal synaptic organization highlighting the potential of gamma stimulation as a therapeutic strategy for cognitive deficits in individuals with DS. Future studies will be needed to explore the effects in female mice as well as to investigate if longer multisensory 40 Hz treatment and/or earlier treatment onset, such as in the early post-natal stage, or addition of other sensory modalities (e.g., tactile stimulation) will further increase these treatment benefits.

Materials and Methods

Animals

All animal work was approved by the Committee for Animal Care of the Division of Comparative Medicine at the Massachusetts Institute of Technology and by the Institutional Animal Care (MIT-CAC, approval number: 0621-033-24). Male Ts65Dn mice aged 6-8 months were used for all experiments. Mice were housed in groups no larger than five on a standard 12-h light/12-h dark

279 cycle; all experiments were performed during the light cycle. Food and water were provided
280 without restriction. For all experiments, mice from the same litter were divided into different
281 conditions, respectfully. If additional groups were added, respective ambient groups were always
282 repeated concurrently. For tissue collection, mice were anesthetized with isoflurane and cardiac
283 perfused with ice cold DPBS (Thermo Fisher Scientific, 14190235).
284
285 **Concurrent 40 Hz auditory and visual stimulation protocol**
286 Light flicker stimulation was delivered as previously described [10,51]. Mice were transported from
287 the holding room to a separate stimulation room, located on another floor. Mice were habituated
288 under dim light for 30 min before the start of the experiment, and then introduced to the stimulation
289 cage (like the home cage, except without bedding and three of its sides covered with black
290 sheeting). All sensory gamma stimulation protocols were administered daily for 1h/d for the
291 number of days as specified. Mice were exposed to one of two stimulations: dark/quiet or
292 concurrent 40 Hz light flicker and auditory tone for one hour per day. Mice were allowed to freely
293 move inside the cage but did not have access to food or water during the 1-hour stimulation period.
294 An array of light emitting diodes (LEDs) was present on the open side of the cage and was driven
295 to flicker at a frequency of 40 Hz with a square wave current pattern and 50% duty cycle using an
296 Arduino system. The luminescence intensity of light that covered inside the total area of
297 multisensory stimulation cage varied from ~ 200 – 1000 lux as measured from the back and front
298 of the cage (mice were free to move in the cage). For audio stimulation, a 10 kHz tone at 60 dB
299 was played at 40 Hz with a 4% duty cycle from a speaker located above the stimulation cages.
300 After 1h of stimulation, mice were returned to their home cage and allowed to rest for a further 30
301 min before being transported back to the holding room. Ambient mice group underwent the same
302 transport and were exposed to similar cages with similar food and water restriction in the same
303 room but experienced only normal room light and natural environmental noise for the 1h duration.
304
305 **Behavior**
306 Behavioral protocols were conducted towards the end of the 3-weeks stimulation protocol. Ethanol
307 was used to wipe down all testing apparatuses between uses.
308 Novel Object Recognition
309 The novel object recognition (NOR) task consisted of a habituation phase followed by training and
310 testing performed the following day, as previously described [52]. 24 hours before training, mice
311 were habituated to an open testing arena (40 cm L x 40 cm W x 35 cm H) for 10 min, during which
312 total distance (cm), time in the center (s), and velocity (cm/s) were calculated (TSE Systems) to
313 evaluate open field behavior. During training, mice were placed into the same box with two
314 identical objects placed in opposite corners. Mice were allowed a total of 20 s of object interaction
315 time (within a maximum time frame of 10 minutes), and then immediately removed from the arena.
316 Object memory was tested 1 hour later using the same procedure during training, except one object
317 was replaced with a novel one in its place. Object exploration was recorded when the snout
318 contacted either object and was calculated by a recognition index, RI =

319 (Tnovel/(Tnovel+Tfamiliar)) x100, where Tnovel and Tfamiliar indicate the time spent with the
320 novel and familiar object, respectively.
321 Novel Object Location
322 The novel location recognition (NOL) task was performed using the same procedure as the object
323 recognition task, except two identical objects were used for both training and testing, and one
324 object was displaced to a novel location during testing.
325
326 Spontaneous Alternation
327 A Y-maze was used for testing with an apparatus with three equal arms (30 cm length, 10 cm
328 width, and 20 cm height) placed 120º apart, made of opaque acrylic glass. A mouse was placed at
329 the maze center and was allowed 7-min of exploration of the environment. An arm entry was
330 scored when the mouse entered the arm with all four paws. Total number of entries (N) and number
331 of 'correct' triplets (M, consecutive choices of each of the three arms without re-entries) was
332 evaluated. The alternation rate was computed according to the formula: R (%)=(M/(N-2))x100.
333
334 **Single-nucleus RNA sequencing**
335 24 hours after the final stimulation session, the hippocampi of the mice were dissected and snap
336 frozen in liquid nitrogen and stored at −80 °C. The protocol for the isolation of nuclei from frozen
337 brain tissue was adapted from a previous study [53]. All procedures were carried out on ice. Briefly,
338 two mouse hippocampi were pooled per sample (3 samples per condition) and homogenized in 1
339 ml homogenization buffer (320 mM sucrose, 5 mM CaCl2, 3 mM Mg (CH3COO)2, 10 mM Tris
340 HCl pH 7.8, 0.1 mM EDTA pH 8.0, 0.1% IGEPAL CA-630, 1 mM β-mercaptoethanol, and 0.4 U
341 µl-1 recombinant RNase inhibitor (Clontech) using a Wheaton Dounce tissue grinder. The
342 homogenized tissue was filtered through a 40-µm cell strainer, mixed with an equal volume of
343 working solution (50% OptiPrep density gradient medium (Sigma-Aldrich), 5 mM CaCl2, 3 mM
344 Mg(CH3COO)2, 10 mM Tris HCl pH 7.8, 0.1 mM EDTA pH 8.0, and 1 mM β-mercaptoethanol)
345 and loaded on top of an OptiPrep density gradient (29% OptiPrep solution (29% OptiPrep density
346 gradient medium,134 mM sucrose, 5 mM CaCl2, 3 mM Mg(CH3COO)2, 10 mM Tris HCl pH 7.8,
347 0.1 mM EDTA pH 8.0, 1 mM β-mercaptoethanol, 0.04% IGEPAL CA-630, and 0.17 U µl-1
348 recombinant RNase inhibitor) on top of 35% OptiPrep solution (35% OptiPrep density gradient
349 medium, 96 mM sucrose, 5 mM CaCl2, 3 mM Mg(CH3COO)2, 10 mM Tris HCl pH 7.8, 0.1 mM
350 EDTA pH 8.0, 1 mM β-mercaptoethanol, 0.03% IGEPAL CA-630, and 0.12 U µl-1 recombinant
351 RNase inhibitor). The nuclei were separated by ultracentrifugation using an SW32 rotor (5 min,
352 10,000xG, 4°C). Nuclei were collected from the 29%/35% interphase, washed with PBS
353 containing 0.04% BSA, centrifuged at 300g for 3 min (4 °C), and washed with 1 ml of PBS
354 containing 1% BSA. The nuclei were counted and diluted to a concentration of 1,000 nuclei per
355 microliter in PBS containing 1% BSA. Libraries were prepared using the Chromium Single Cell
356 3′ Reagent Kits v.3.1 (Dual Index) according to the manufacturer's protocol (10X Genomics,
357 Pleasanton, CA). The snRNA-seq libraries were sequenced using NextSeq 500/550 High Output
358 (150 cycles).

Single nuclei RNA-seq data analysis

Data preprocessing, differential expression, gene ontology analyses

Gene counts were retrieved by mapping raw reads to the mouse genome (mm10) using CellRanger software (v 7.0.1). Initial preprocessing of the samples (e.g., removal of ambient noise, identification and removal of contamination from adjacent brain regions, and stressed or damaged cell and low quality cells) were performed using ACTIONet[54]. Downstream analysis was performed in Seurat (v 4.3.0). Nuclei with a minimum 500 unique molecular identifiers (UMIs) and less than 5% mitochondrial genes were considered for downstream analysis. Doublets were identified and removed using scds (v 1.10.0) and genes with no expression was discarded. Count data were log-normalized using NormalizeData and top 2000 highly variable genes were determined using FindVariableFeatures. Expression of these genes were subsequently used to scale gene expression to zero mean and unit variance with ScaleData function. Scaled data was further regressed out for mitochondrial percentage. Top 75 principal components were estimated using RunPCA and aligned with Harmony to account for technical batch effects considering individual sample as batch. Optimum number of principle components (PCs) were determined based on the ElbowPlot and the first 16 PCs was used as input for downstream analyses. A neighborhood graph was constructed based on the Euclidean distance metric in the adjusted PC space using FindNeighbors, and nuclei were clustered using the Louvain method in FindClusters at resolution 0.2. RunUMAP functions with min.dist = 0.5 and spread = 0.5 were used to calculate two-dimensional UMAP coordinates and nuclei clusters were visualized using DimPlot. Cell type specific clusters were annotated using canonical markers. Nuclei clusters expressing mixed cell type specific markers were discarded. Cell type specific marker genes were identified based on the differential expression of each cell type against all other cell types using FindMarkers and genes with significance (adjusted P value<0.05) and increased expression were only considered for cell type specific markers. Differential gene expression analysis was performed using MAST (v 1.20.0). Genes with log2 fold change >0.1 and adjusted p value <0.05 were defined as differentially expressed. Module score was calculated using AddModuleScore in Seurat. Gene ontology analyses were performed using either Gene ontology (http://geneontology.org) or Metascape (https://www.metascape.org/). For supervised GO module analysis particularly for oxidative phosphorylation (GO:0006119) and cellular respiration (GO:0045333), we retrieved genes related to these GO terms using gconvert function of gprofiler2 (v 0.2.1). Co-expression GO module score was calculated using AddModuleScore function in Seurat.

Weighted gene co-expression analysis

Weighted gene co-expression analysis (WGCNA) was performed as previously described in [55–57]. Briefly, “metacells” were constructed computing mean expression from 25 neighbors using k-nearest neighbors. Normalized and scaled metacells were then used to calculate pair-wise correlations between all gene pairs. Subsequently, based on the approximate scale-free topology, a threshold power of 4 was selected to emphasize the stronger correlations and to compute pair-wise topological overlap to construct a signed network. Modules with minimum size of 25 and

399 deep split of 4 were used for the analysis. Closely related modules were merged using dissimilarity
400 correlation threshold of 0.2. Modules were summarized as network of modular eigengenes (MEs),
401 which was defined based on the first major component of the module and used to compare between
402 the two groups. Module membership of genes was defined as the correlation of gene expression
403 profile with MEs. Hub genes were defined based on the intra-modular connectivity (kME) and top
404 25 hub genes were plotted using igraph package (v 1.3.1). Association between hub module genes
405 and transcription factors was analyzed using ChEA3[58].
406
407 Analyses of granule cells
408 To select granule cells (GCs) we first filtered the snRNA-seq data based on the expression level
409 of Prox1, which is a pan GC marker. Only cells with an expression level of Prox1 greater than 1
410 were retained for subsequent analyses. Cells were normalized, scaled, harmonized and top 30
411 components were used to construct cell clusters and UMAP at resolution of 0.8. Cluster specific
412 marker genes were defined using FindAllMarkers (only.pos = TRUE, min.pct = 0.25, assay =
413 "RNA") and top 200 genes were used to perform gene enrichment analyses with granule cell
414 specific markers defined in the previous study [59]. Based on the enrichment results, cell clusters
415 were annotated into glial (radial glial), and granule cells (neuroblasts, mature and immature).
416 Clusters that did not show overlap to the marker genes were labeled as unknown cluster type.
417 Annotated granule cells (immature, mature, neuroblasts) were considered for downstream analyses
418 and pseudotime analysis was performed using Monocle. Briefly, we kept the original clustering
419 and dimension reduction from Seurat and created a Monocle cell data set (CDS) using the
420 new_cell_data_set function and treated all cells as a single partition. For trajectory analysis,
421 learn_graph function was used to learn the trajectory graph of the cells. Cells were subsequently
422 assigned a pseudotime value based on their projection on the principal graph learned in
423 the learn_graph function and order_cells function was used to order cells along the trajectory. To
424 find genes whose expression changes along the pseudotime, we then applied a generalized additive
425 model along the principal trajectory via graph_test function. Genes with q-value less than 0.05
426 were considered only for downstream analysis. Top 100 pseudotime associated genes were
427 visualized as heatmap using Heatmap function. Genes that are differentially expressed between
428 ambient and stimulation groups along the trajectory were determined using fit_models with q-
429 value cutoff set at 0.05. Gene ontology analysis was performed using Metascape and
430 ClusterProfiler.
431
432 Analyses of published datasets
433 Hippocampal bulk RNA-seq raw data pertaining to 4, 8, 12 and 18 months of wild type mice were
434 retrieved from GSE168137 and analyzed. Single cell RNA-seq data from frontal cortex and
435 striatum of 4 weeks and 90 weeks of mice was retrieved from GSE207848 and processed in house.
436 List of downregulated genes in excitatory neurons of old individuals compared to young subjects
437 were retrieved from AgeAnno [60]. Cortical and hippocampal bulk RNA-seq data related to Ts65Dn
438 and littermate controls were downloaded from GSE213500 and processed in house. List of

439 downregulated genes in the excitatory neurons of prefrontal cortex from patients with Down
440 syndrome was retrieved from the provided supplementary file in [61]. Bulk RNA-seq data related to
441 5xFAD and wild type mice of 4 and 8 months were downloaded from GSE168137 and analyzed
442 in house. Single cell data related to 5xFAD and wild type mice of 7 months old were retrieved
443 from GSE140511 and processed in house. Hippocampal excitatory neuronal transcriptomic data
444 from individuals with Alzheimer´s disease and controls were provided by Mathys et al., (in
445 review). For Bulk RNA-seq data, genes with low no expression were removed. Differential
446 expression analysis was performed using DESeq2 (v 1.34.0). Genes with FDR<0.05 were defined
447 as differentially expressed. For single cell data related to aging and AD, data were processed as
448 described above using Seurat and cell clusters were visualized in UMAP space. Cell clusters
449 enriched for Slc17a7/VGLUT1, marker for excitatory neuron, were further analyzed for
450 differential expression analysis. Differentially expressed genes (FDR <0.05, abs(log2FC)>0.1) in
451 the SLC7A7+ human hippocampal snRNA-seq data were determined after adjusting for age, sex,
452 and post-mortem interval. Differential expression analyses were performed using MAST. Module
453 score in bulk RNA-seq data was computed using svd as implemented in moduleEigengene of
454 WGCNA package. Hypergeometric overlap analysis was performed using GeneOverlap package
455 in R.
456
457
458 **Immunohistochemistry**
459 24 hours after the final stimulation session, mice were transcardially perfused with 40 ml of ice-
460 cold phosphate buffered saline (PBS) followed by 40 ml of 4% paraformaldehyde (PFA) in PBS.
461 Brains were removed and post-fixed in 4% PFA overnight at 4°C and transferred to PBS prior to
462 sectioning. Brains were sectioned 40 µm thick with a Leica VT1000S vibratome (Leica). Sections
463 were permeabilized and blocked in PBS with 0.3% Triton X-100 and 10% donkey serum at room
464 temperature for 2-hrs. Sections were incubated overnight at 4°C in primary antibody containing
465 PBS with 0.3% Triton X-100 and 10% donkey serum. Primary antibodies were anti-synaptophysin
466 (Synaptic Systems, 101004), anti-PSD95 (Abcam, ab18258), anti-Ki67 (Abcam, ab15580), anti-
467 cFos (Santa Cruz Biotech, sc-166940), anti-Reelin (Millipore Sigma, MAB5364), anti-TCF4
468 (Protein Tech, 13838-1-AP), anti-NeuN (Synaptic Systems, 266004). The following day, brain
469 sections were incubated with fluorescently conjugated secondary antibodies (Jackson
470 ImmunoResearch) for 2 hours at room temperature, and nuclei were stained with DAPI
471 (Invitrogen, D1306). Images were acquired using a confocal microscope (LSM 710; Zeiss or LSM
472 900; Zeiss).
473
474 EdU Staining
475 EdU staining was conducted using the Click-iT™ EdU imaging kit (ThermoFisher, C10340)
476 according to the manufacturer's protocol. This protocol is normally intended for use in cell culture
477 but was adapted for histological staining of brain tissue. Each mouse was intraperitoneally injected
478 with EdU 25 mg/kg for 2 days prior to perfusion. Slides containing mounted frozen brain sections

479 were allowed to thaw to room temperature and then fixed with 4% paraformaldehyde in phosphate
480 buffer saline (PBS) for 15 min. After washing twice with 3% bovine serum albumin (BSA) in PBS,
481 the sections were permeablized with 0.5% Triton X-100 in PBS for 20 min. The sections were
482 again washed twice with 3% BSA in PBS and then incubated with a Click-iT™ reaction cocktail
483 containing Click-iT™ reaction buffer, $CuSO_4$, Alexa Fluor® 594 Azide, and reaction buffer
484 additive for 30 min while protected from light. The sections were washed once more with 3% BSA
485 in PBS before being mounted and imaged.
486
487 **Image analysis**
488 c-Fos quantification
489 Images acquired at 63x magnification were analyzed in CellProfiler (v 4.2.5). Briefly, after
490 intensity scaling and smoothing of c-Fos signals, images were then processed to apply
491 EnhanceOrSuppressFeatures function to enhance the visibility of c-Fos signals. This was followed
492 by the application of a threshold using Threshold function. Subsequently, regions of interest
493 (ROIs) were drawn, and primary objects were identified using IdentifyPrimaryObjects function.
494 The following parameters were used for this purpose: diameter of objects in pixel units: 48-200,
495 threshold strategy: Global, thresholding method: Otsu, two classes thresholding, thresholding
496 smoothing scale: 1, threshold correction factor: 0.1, lower and upper bounds on threshold: 0.1-1,
497 method to distinguish clumped objects: shape, method to draw dividing lines between clumped
498 objects: shape, discarded objects outside the diameter range, but not those touching the border of
499 the image. MeasureObjectSizeShape function was then applied to quantify the total number of
500 objects in each image. Representative images were acquired using 20x objective and highlight c-
501 Fos expression at the granule cell molecular layer of the hippocampal dentate gyrus in FigS2.
502
503 Quantification of colocalization of synaptophysin and PSD95
504 Following the image acquisition using 63x objective, files were imported into Imaris (v9.9). First,
505 the Spots feature of the software was utilized to detect PSD95 and synaptophysin puncta. For each
506 fluorescence channel, minimum and maximum intensity values were collected from every image
507 to maximize detection of puncta and minimize background noise. Means calculated from these
508 minimum and maximum intensity values became the intensity thresholds for the Spots applied to
509 every image. The Spots using the cohort's shared threshold values were applied to one sample
510 image, then saved as a Macro and applied to all other images. After applying Spots, the
511 colocalization function was executed to mark and quantify points from each Spots channel that
512 were within 2um of each other. To validate this proxy method for quantifying mature functional
513 synapses, another method for colocalization analysis was also executed. To do this, the Imaris
514 software's Colocalization Channel function was used. Minimum and maximum thresholds were
515 once again collected from each fluorescence channel to build the new colocalization channel. After
516 calculating the means of the threshold values in each, the channel was built and manually added
517 to every image file. Spots were then added to the new channel to register and quantify the
518 colocalized points detected. Data was analyzed from both methods of analysis to confirm trend.

To quantify Reln+ neurons, brain slices (3-5 technical replicates/mouse) were immunostained with anti-Reelin, anti-NeuN and DAPI and images were acquired using the 20x objective in LSM 900. Image analysis was performed using Imaris (v9.9). First, we created surfaces for Reln and NeuN individually. Then, we counted the number of Reln surfaces that overlapped with those of NeuN to identify Reln+ neurons. We calculated the ratio of Reln+ neurons to the total number of neurons to determine the proportion of Reln+ neurons.

To investigate TCF4 expression changes between the two groups, we performed immunostaining experiment using anti-TCF4 and DAPI on brain slices and acquired images (20x, LSM900) from the dentate gyrus of the hippocampus. To ensure reproducibility, experiment was repeated three times for each mouse. For TCF4 mean intensity analysis, we used the Measure function in ImageJ software (v2.14.0/1.54f). To minimize the technical bias, we averaged the TCF4 intensity across all replicates for each mouse and normalized it to the mean DAPI signal for all control samples.

Statistical Analyses

Statistical analysis was conducted in R (v 4.1.2) or Prism (v 8). Statistical details of the experiments, including the statistical tests used, exact value of n, definition of measures can be found in the corresponding figure legends. Unless otherwise stated, statistical significance was set at 0.05.

Acknowledgements

We are thankful to Dr Nancy Kopell, Dr Michelle McCarthy and Tsai lab members for their helpful comments during preparation of this manuscript. We are grateful to the following individuals and groups for their kind contributions and support of this work: the Alana USA Foundation, Inc, National Science Foundation Graduate Research Fellowship under Grant No.1122374. MRI is a EMBO long term postdoctoral fellow.

Author contributions

MRI, BJ, and L-HT conceptualized the study. BJ performed behavioral experiments, analyzed data, and interpreted results. MRI analyzed sequencing data, interpreted results, and made figures. BS, MM, NT, DSP, DRA, FJ, CA, VF performed experiments. SSP performed initial preprocessing of sequencing data. MK and ESB provided tools. L-HT provided tools and supervised all aspects of the project. MRI, UG, BJ, and L-HT wrote the manuscript based on inputs from all authors.

Declaration of Interests

L-HT and ESB are scientific co-founders and serve on the scientific advisory board of Cognito Therapeutics.

Data Availability

All data necessary for the conclusion of this study are presented in the manuscript. Publicly available sequencing data used in this study are GSE168137, GSE207848, GSE213500, GSE168137, and GSE140511. Both raw and processed sequencing data from this study have been deposited at GEO and are publicly available as of the date of publication.

References

1. Guidi, S. *et al.* Neurogenesis impairment and increased cell death reduce total neuron number in the hippocampal region of fetuses with Down syndrome. *Brain Pathol. Zurich Switz.* **18**, 180–197 (2008).
2. Hanson, J. E., Blank, M., Valenzuela, R. A., Garner, C. C. & Madison, D. V. The functional nature of synaptic circuitry is altered in area CA3 of the hippocampus in a mouse model of Down's syndrome. *J. Physiol.* **579**, 53–67 (2007).
3. Pennington, B. F., Moon, J., Edgin, J., Stedron, J. & Nadel, L. The neuropsychology of Down syndrome: evidence for hippocampal dysfunction. *Child Dev.* **74**, 75–93 (2003).
4. Tungate, A. S. & Conners, F. A. Executive function in Down syndrome: A meta-analysis. *Res. Dev. Disabil.* **108**, 103802 (2021).
5. Hithersay, R. *et al.* Association of Dementia With Mortality Among Adults With Down Syndrome Older Than 35 Years. *JAMA Neurol.* **76**, 152–160 (2019).
6. Martorell, A. J. *et al.* Multi-sensory Gamma Stimulation Ameliorates Alzheimer's-Associated Pathology and Improves Cognition. *Cell* **177**, 256-271.e22 (2019).
7. Adaikkan, C. *et al.* Gamma Entrainment Binds Higher-Order Brain Regions and Offers Neuroprotection. *Neuron* **102**, 929-943.e8 (2019).
8. Chan, D. *et al.* Gamma frequency sensory stimulation in mild probable Alzheimer's dementia patients: Results of feasibility and pilot studies. *PLOS ONE* **17**, e0278412 (2022).
9. Murdock, M. H. *et al.* Multisensory gamma stimulation promotes glymphatic clearance of amyloid. *Nature* **627**, 149–156 (2024).
10. Iaccarino, H. F. *et al.* Gamma frequency entrainment attenuates amyloid load and modifies microglia. *Nature* **540**, 230–235 (2016).
11. He, Q. *et al.* A feasibility trial of gamma sensory flicker for patients with prodromal Alzheimer's disease. *Alzheimers Dement. N. Y. N* **7**, e12178 (2021).
12. Liu, C. *et al.* Modulating Gamma Oscillations Promotes Brain Connectivity to Improve Cognitive Impairment. *Cereb. Cortex* **32**, 2644–2656 (2022).
13. Cimenser, A. *et al.* Sensory-Evoked 40-Hz Gamma Oscillation Improves Sleep and Daily Living Activities in Alzheimer's Disease Patients. *Front. Syst. Neurosci.* **15**, 746859 (2021).
14. Guerra, A. *et al.* Enhancing Gamma Oscillations Restores Primary Motor Cortex Plasticity in Parkinson's Disease. *J. Neurosci.* **40**, 4788–4796 (2020).
15. Belichenko, P. V. *et al.* Synaptic structural abnormalities in the Ts65Dn mouse model of Down Syndrome. *J. Comp. Neurol.* **480**, 281–298 (2004).
16. Reeves, R. H. *et al.* A mouse model for Down syndrome exhibits learning and behaviour deficits. *Nat. Genet.* **11**, 177–184 (1995).
17. Clark, S., Schwalbe, J., Stasko, M. R., Yarowsky, P. J. & Costa, A. C. S. Fluoxetine rescues deficient neurogenesis in hippocampus of the Ts65Dn mouse model for Down syndrome. *Exp. Neurol.* **200**, 256–261 (2006).
18. Reeves, R. H. *et al.* A mouse model for Down syndrome exhibits learning and behaviour deficits. *Nat. Genet.* **11**, 177–184 (1995).
19. Kleschevnikov, A. M. *et al.* Deficits in Cognition and Synaptic Plasticity in a Mouse Model of Down Syndrome Ameliorated by GABAB Receptor Antagonists. *J. Neurosci.* **32**, 9217–9227 (2012).

20. Faizi, M. *et al.* Comprehensive behavioral phenotyping of Ts65Dn mouse model of Down Syndrome: Activation of β1-adrenergic receptor by xamoterol as a potential cognitive enhancer. *Neurobiol. Dis.* **43**, 397–413 (2011).
21. Chung, L. A Brief Introduction to the Transduction of Neural Activity into Fos Signal. *Dev. Reprod.* **19**, 61–67 (2015).
22. Koopmans, F. *et al.* SynGO: An Evidence-Based, Expert-Curated Knowledge Base for the Synapse. *Neuron* **103**, 217-234.e4 (2019).
23. Cingolani, L. A. & Goda, Y. Actin in action: the interplay between the actin cytoskeleton and synaptic efficacy. *Nat. Rev. Neurosci.* **9**, 344–356 (2008).
24. Mei, L. & Xiong, W.-C. Neuregulin 1 in neural development, synaptic plasticity and schizophrenia. *Nat. Rev. Neurosci.* **9**, 437–452 (2008).
25. Yasuda, R., Hayashi, Y. & Hell, J. W. Camkii: A Central Molecular Organizer of Synaptic Plasticity, Learning and Memory. *Nat. Rev. Neurosci.* **23**, 666–682 (2022).
26. Holahan, M. R., Honegger, K. S., Tabatadze, N. & Routtenberg, A. GAP-43 gene expression regulates information storage. *Learn. Mem.* **14**, 407–415 (2007).
27. Doze, V. A. *et al.* Long-term α1A-adrenergic receptor stimulation improves synaptic plasticity, cognitive function, mood, and longevity. *Mol. Pharmacol.* **80**, 747–758 (2011).
28. Egan, M. F. *et al.* Variation in *GRM3* affects cognition, prefrontal glutamate, and risk for schizophrenia. *Proc. Natl. Acad. Sci.* **101**, 12604–12609 (2004).
29. Bernal, J. Thyroid hormone receptors in brain development and function. *Nat. Clin. Pract. Endocrinol. Metab.* **3**, 249–259 (2007).
30. Cheadle, L. & Biederer, T. The novel synaptogenic protein Farp1 links postsynaptic cytoskeletal dynamics and transsynaptic organization. *J. Cell Biol.* **199**, 985–1001 (2012).
31. Lee, J.-R. Protein tyrosine phosphatase PTPRT as a regulator of synaptic formation and neuronal development. *BMB Rep.* **48**, 249–255 (2015).
32. Choi, Y. *et al.* NGL-1/LRRC4C Deletion Moderately Suppresses Hippocampal Excitatory Synapse Development and Function in an Input-Independent Manner. *Front. Mol. Neurosci.* **12**, 119 (2019).
33. Akaneya, Y. *et al.* Ephrin-A5 and EphA5 interaction induces synaptogenesis during early hippocampal development. *PloS One* **5**, e12486 (2010).
34. Herring, A. *et al.* Reelin depletion is an early phenomenon of Alzheimer's pathology. *J. Alzheimers Dis. JAD* **30**, 963–979 (2012).
35. Kocherhans, S. *et al.* Reduced Reelin expression accelerates amyloid-beta plaque formation and tau pathology in transgenic Alzheimer's disease mice. *J. Neurosci. Off. J. Soc. Neurosci.* **30**, 9228–9240 (2010).
36. Marckx, A. T., Fritschle, K. E., Calvier, L. & Herz, J. Reelin changes hippocampal learning in aging and Alzheimer's disease. *Behav. Brain Res.* **414**, 113482 (2021).
37. Lopera, F. *et al.* Resilience to autosomal dominant Alzheimer's disease in a Reelin-COLBOS heterozygous man. *Nat. Med.* **29**, 1243–1252 (2023).
38. Shariq, M. *et al.* Adult neural stem cells have latent inflammatory potential that is kept suppressed by *Tcf4* to facilitate adult neurogenesis. *Sci. Adv.* **7**, eabf5606 (2021).
39. Habib, N. *et al.* Div-Seq: Single-nucleus RNA-Seq reveals dynamics of rare adult newborn neurons. *Science* **353**, 925–928 (2016).
40. Zhou, Y. *et al.* Molecular landscapes of human hippocampal immature neurons across lifespan. *Nature* **607**, 527–533 (2022).
41. Cembrowski, M. S., Wang, L., Sugino, K., Shields, B. C. & Spruston, N. Hipposeq: a comprehensive RNA-seq database of gene expression in hippocampal principal neurons. *eLife* **5**, e14997 (2016).
42. Dupret, D. *et al.* Spatial relational memory requires hippocampal adult neurogenesis. *PloS One* **3**, e1959 (2008).
43. Berdugo-Vega, G. *et al.* Increasing neurogenesis refines hippocampal activity rejuvenating navigational learning strategies and contextual memory throughout life. *Nat. Commun.* **11**, 135 (2020).

44. Bianchi, P. *et al.* Early pharmacotherapy restores neurogenesis and cognitive performance in the Ts65Dn mouse model for Down syndrome. *J. Neurosci. Off. J. Soc. Neurosci.* **30**, 8769–8779 (2010).
45. Goldberg, M. *et al.* Exercise as a model to identify microRNAs linked to human cognition: a role for microRNA-409 and microRNA-501. *Transl. Psychiatry* **11**, 1–13 (2021).
46. Fischer, A., Sananbenesi, F., Wang, X., Dobbin, M. & Tsai, L.-H. Recovery of learning and memory is associated with chromatin remodelling. *Nature* **447**, 178–182 (2007).
47. Contestabile, A. *et al.* Lithium rescues synaptic plasticity and memory in Down syndrome mice. *J. Clin. Invest.* **123**, 348–361 (2013).
48. Fernandez, F. *et al.* Pharmacotherapy for cognitive impairment in a mouse model of Down syndrome. *Nat. Neurosci.* **10**, 411–413 (2007).
49. Parrini, M. *et al.* Aerobic exercise and a BDNF-mimetic therapy rescue learning and memory in a mouse model of Down syndrome. *Sci. Rep.* **7**, 16825 (2017).
50. Zhou, W.-B. *et al.* Luteolin induces hippocampal neurogenesis in the Ts65Dn mouse model of Down syndrome. *Neural Regen. Res.* **14**, 613–620 (2019).
51. Singer, A. C. *et al.* Noninvasive 40-Hz light flicker to recruit microglia and reduce amyloid beta load. *Nat. Protoc.* **13**, 1850–1868 (2018).
52. Leger, M. *et al.* Object recognition test in mice. *Nat. Protoc.* **8**, 2531–2537 (2013).
53. Mathys, H. *et al.* Single-cell transcriptomic analysis of Alzheimer's disease. *Nature* **570**, 332–337 (2019).
54. Mohammadi, S., Davila-Velderrain, J. & Kellis, M. A multiresolution framework to characterize single-cell state landscapes. *Nat. Commun.* **11**, 5399 (2020).
55. Islam, M. R. *et al.* A microRNA signature that correlates with cognition and is a target against cognitive decline. *EMBO Mol. Med.* **13**, e13659 (2021).
56. Morabito, S. *et al.* Single-nucleus chromatin accessibility and transcriptomic characterization of Alzheimer's disease. *Nat. Genet.* **53**, 1143–1155 (2021).
57. Morabito, S., Reese, F., Rahimzadeh, N., Miyoshi, E. & Swarup, V. hdWGCNA identifies co-expression networks in high-dimensional transcriptomics data. *Cell Rep. Methods* **3**, 100498 (2023).
58. Keenan, A. B. *et al.* ChEA3: transcription factor enrichment analysis by orthogonal omics integration. *Nucleic Acids Res.* **47**, W212–W224 (2019).
59. Hochgerner, H., Zeisel, A., Lönnerberg, P. & Linnarsson, S. Conserved properties of dentate gyrus neurogenesis across postnatal development revealed by single-cell RNA sequencing. *Nat. Neurosci.* **21**, 290–299 (2018).
60. Huang, K. *et al.* AgeAnno: a knowledgebase of single-cell annotation of aging in human. *Nucleic Acids Res.* **51**, D805–D815 (2023).
61. Palmer, C. R., Liu, C. S., Romanow, W. J., Lee, M.-H. & Chun, J. Altered cell and RNA isoform diversity in aging Down syndrome brains. *Proc. Natl. Acad. Sci. U. S. A.* **118**, e2114326118 (2021).

Figure Legends

Fig 1. Multisensory gamma stimulation improves spatial working memory in Ts65Dn mice. A) Experimental scheme. B) Novel Object Recognition (NOR) test. Quantification of recognition index during NOR. C) Novel Object Location (NOL) test. Quantification of recognition index during NOL. D) Spontaneous alteration based on Y-maze. Quantification of percent alteration and total number of entries. ambient = 12, stimulation = 12, unpaired t-test, two-tailed, *P<0.05, ****P<0.0001. Error bars indicate mean ± standard error mean.

Fig 2. Molecular signatures underlying multisensory gamma stimulation-associated cognitive benefits in the hippocampus. A) Experimental scheme for the single nuclei RNA-seq experiment in Ts65Dn mice B) Unbiased clustering of hippocampal snRNA-seq data for 15884 nuclei represented on a UMAP. Cell types are annotated based on the marker genes. Ex: Excitatory Neurons, Astro: Astrocytes, Oligo: Oligodendrocytes, In: Inhibitory Neurons, OPC: Oligodendrocyte precursor cells, Micro: Microglia. C) Heatmap showing number of differentially expressed genes in excitatory and inhibitory neurons in the hippocampal snRNA-seq data from stimulation vs ambient Ts65Dn mice. D) Gene ontology analyses for the upregulated and downregulated genes in hippocampal excitatory and inhibitory neurons in stimulation vs ambient Ts65Dn mice. Color represents statistical significance after multiple testing adjustment. E) Signed bar plot displaying significant co-expression changes of the identified 7 gene modules in hippocampal excitatory neurons in stimulation vs ambient TsD65n mice. Red color denotes increased and blue color decreased expression in stimulated mice. X-axis represents signed -log10 p value. F) Hub genes of modules Ex-3, Ex-6 and Ex-7. G) Top gene ontology biological processes for modules Ex-3, Ex-6, and Ex-7. H) Quantification of mature synapses in granule cell molecular layer of dentate gyrus in stimulation and ambient Ts65Dn mice via co-localization of PSD95 and synaptophysin. Representative images of mouse brain slices stained with PSD95, synaptophysin and DAPI. Images were acquired using 63x objective. Triangles indicate colocalized puncta. Scale bar = 10 microns. t-test, two-tailed, unpaired, *P<0.05. Error bars indicate mean ± sem. ambient = 6, stimulation = 7 mice. I) Hub genes overlapping with disease risk genes for Alzheimer´s disease. J) Quantification of *Reln*+ neurons after ambient or 40Hz stimulation. Representative confocal images of hippocampal CA3 area brain slices from Ts65Dn mice after staining for Reelin and NeuN with DAPI counterstain. Merged panel shows all three markers. 20x objective. Scale bar = 50 pixels. Bar plots show mean proportion of *Reln*+ neurons between the ambient and stimulation groups. Error bars indicate mean ± sem. t-test, two-tailed, unpaired, **P<0.01. Number of mice = 5/group. K-L) Hypergeometric overlap of the genes in modules Ex-3, Ex-6, and Ex-7 with different sets of downregulated genes related to (K) aging and (L) Alzheimer's disease (AD). Color represents fold enrichment. *FDR<0.05, **FDR<0.01, ***FDR<0.001.

743 **Fig 3. Multisensory gamma stimulation increases adult neurogenesis in Ts65Dn mice.**
744 A) Top 10 ranked TFs for module Ex-7. Color represents -log10 enrichment score based on ChEA3
745 analysis. B) Mean TCF4 fluorescence intensity after treatment of mice with or without 40Hz
746 stimulation. Representative images of TS65Dn mouse brain slices from the hippocampal dentate
747 gyrus area after staining for TCF4 (green) and DAPI (blue). Merged panel shows both markers.
748 Scale bar = 20 microns. Bar plots show normalized mean intensity (% of ambient group) between
749 the two groups. t-test, two-tailed, unpaired. *P<0.05. number of mice = 5/group. C) Sub clusters
750 of immature granule cells represented on a UMAP D) Dot plots showing relative enrichment of
751 marker genes across the three sub-clusters of immature granule cells (GC) E) UMAP plots
752 separated by group reveal differential numbers of cluster 3 immature GC in stimulation group. F)
753 Box plot shows increased proportion of Prox1+ immature GC cells in stimulation vs ambient
754 Ts65Dn mice. Center line represents median; lower and the upper lines represent the 25th and 75th
755 percentiles, respectively; whiskers indicate the smallest and largest values in the 1.5x interquartile
756 range. G-H) Increased cell proliferation in the dentate gyrus of stimulation vs ambient Ts65Dn
757 mice tested via immunolabeling for G) Ki67 (ambient = 6 mice, stimulation = 4 mice); Scale bar
758 = 10 microns. and H) EdU (ambient = 8 mice, stimulation = 8 mice); Scale bar = 50 microns. Error
759 bar indicates mean ± standard error mean. Two tailed, unpaired t-test. *P<0.05, **P<0.01,
760 ***P<0.001.
761
762
763 ## Supplementary Figures
764 **Fig S1. Multisensory gamma stimulation does not affect locomotor and anxiety-like behavior**
765 **in Ts65Dn mice.** A) Quantification of total distance traveled during open field test B)
766 Quantification of time spent in the center. Error bars indicate mean ± standard deviation, unpaired
767 t-test, two-tailed, ambient = 12, stimulation = 12.
768
769 **Fig S2. Multisensory gamma stimulation increases c-Fos positive nuclei in the hippocampus**
770 **of Ts65Dn mice.** A) Experimental outline. B) Representative images of c-Fos expression in the
771 granule cell molecular layer of the dentate gyrus after ambient or 40 Hz stimulation. Magenta
772 represents DAPI and yellow represents c-Fos signals. Scale bar = 50 microns. C) Bar plots show
773 distribution of c-Fos positive nuclei in stimulation group mice relative to the ambient group. N =
774 5 mice /group. Error bar indicates mean ± sem. Two-tailed, unpaired t-test, ***P<0.001.
775
776
777 **Fig S3. Quality control of the hippocampal snRNA-seq data from Ts65Dn mice.** Distribution
778 of A) number of genes B) number of UMI, C) complexity and D) mitochondrial percentage across
779 15884 nuclei. E) Canonical cell type specific marker expression in cognate cell types. Slc17a7,
780 Camk2a in excitatory neurons; Gad1, Gad2 in inhibitory neurons; Pdgfra, Vcan in OPC; Mbp,
781 Plp1 in Oligodendrocytes; Slc1a3, Aqp4 in Astrocytes; Csf1r, Hexb in microglia; Pdgfrb, Cldn5
782 in vascular cells, KI, Slc26a11, Cldn1 in choroid plexus cells. F) Pie chart displaying the

783 distribution of detected cell types. G) Nuclei from stimulation and ambient Ts65Dn mice groups
784 are well integrated. H) Proportion of nuclei detected across cell types in both groups.
785
786 **Fig S4. Top biological processes downregulated in Ts65Dn mice and individuals with DS.** A)
787 Differential gene expression observed in bulk RNA-seq data from hippocampi and cortices of
788 Ts65Dn mice (n = 6) and littermate controls (n = 6). Data were retrieved from GSE213500. Gene
789 counts were normalized and differential expression analysis was performed using DESeq2 after
790 adjusting for region specific difference. B) Gene ontology analyses revealed that the genes related
791 to mRNA processing, synapse organization and cognition are downregulated in Ts65Dn mice
792 compared to the controls. C) GO analysis of genes downregulated in excitatory neurons of *post*
793 *mortem* brains of individuals with DS compared to healthy subjects. Gene expression changes data
794 were retrieved from Palmer CR et al[61].
795
796 **Fig S5. Weighted gene co-expression analysis.** A) Cluster dendrogram for seven excitatory gene
797 modules. B) soft-power threshold was determined based on scale-free topology measure and mean
798 connectivity (see Methods). C) Hub genes of Ex-1 and Ex-2 module.
799
800 **Fig S6. Co-expression pattern of excitatory gene modules along aging.** Expression patterns of
801 module Ex-3, Ex-6 and Ex-7 display reduced co-expression at old age (18 months). Boxplots show
802 changes in gene module expression along aging in the hippocampus. Y-axis shows gene module
803 expression eigenvalue. In the box plots, median is marked with the center line, while the lower and
804 the upper lines represent the 25th and 75th percentiles, respectively. The whiskers indicate the
805 smallest and largest values respectively in the 1.5x interquartile range. P-value determined by
806 Kruskal-Wallis test.
807
808 **Fig S7. Multisensory gamma stimulation increases oxidative phosphorylation in a subset of**
809 **immature granule cells.** A) Heatmap showing relative expression of top 100 genes that
810 significantly changed ($q<0.05$) along the maturation trajectory of granule cells (GC) in stimulation
811 vs ambient Ts65Dn mice B) Biological processes representing differentially expressed genes along
812 the maturation trajectory of GC between the stimulation and ambient groups. C) Biological
813 processes for genes differentially expressed between cluster 1,3 and cluster 2,3.
814
815
816
817

Fig 1

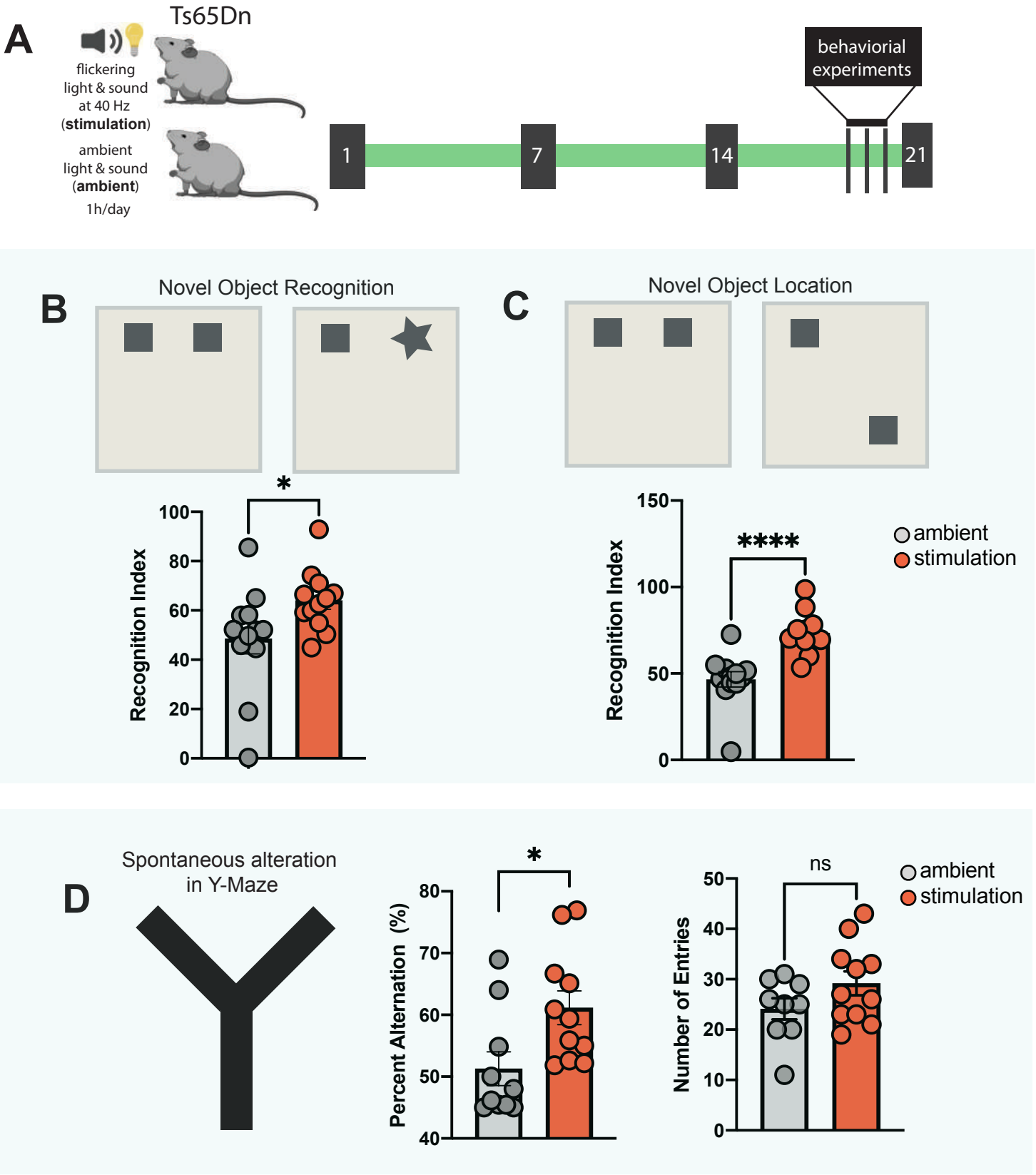
A
Ts65Dn
flickering light & sound at 40 Hz (stimulation)
ambient light & sound (ambient)
1h/day
1
7
14
21
behaviorial experiments
B
Novel Object Recognition
Recognition Index
100
80
60
40
20
0
*
C
Novel Object Location
Recognition Index
150
100
50
0
****
ambient
stimulation
D
Spontaneous alteration in Y-Maze
Percent Alternation (%)
80
70
60
50
40
*
Number of Entries
50
40
30
20
10
0
ns
ambient
stimulation

Fig 2

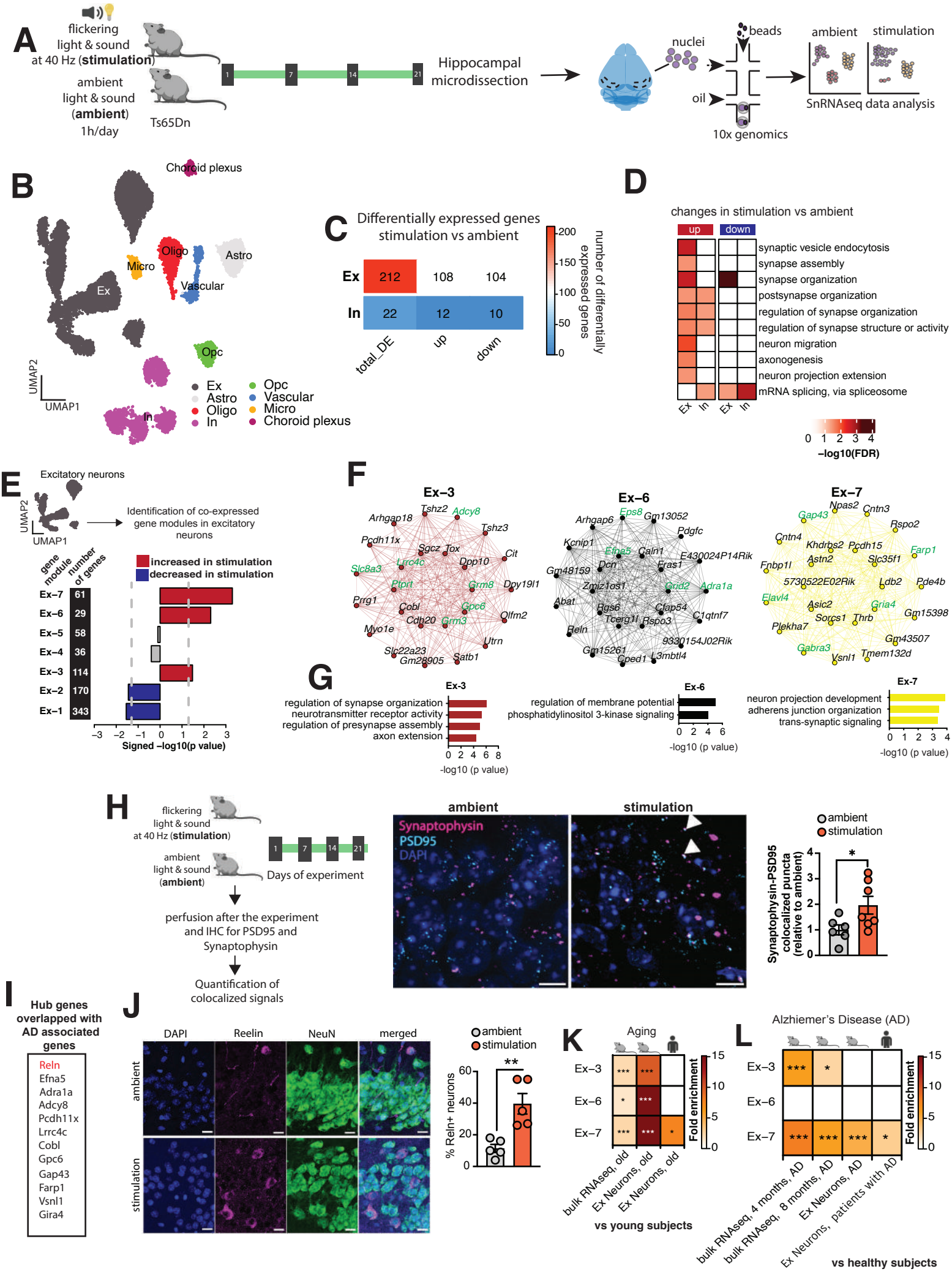
A
flickering light & sound at 40 Hz (stimulation)
ambient light & sound (ambient) 1h/day
Ts65Dn
Hippocampal microdissection
nuclei
beads
oil
10x genomics
ambient
stimulation
SnRNAseq data analysis
B
Choroid plexus
Oligo
Astro
Micro
Vascular
Ex
Opc
In
UMAP2
UMAP1
Ex
Astro
Oligo
In
Opc
Vascular
Micro
Choroid plexus
C
Differentially expressed genes stimulation vs ambient
Ex 212 108 104
In 22 12 10
total_DE
up
down
number of differentially expressed genes
D
changes in stimulation vs ambient
up
down
synaptic vesicle endocytosis
synapse assembly
synapse organization
postsynapse organization
regulation of synapse organization
regulation of synapse structure or activity
neuron migration
axonogenesis
neuron projection extension
mRNA splicing, via spliceosome
Ex In Ex In
–log10(FDR)
E
Excitatory neurons
Identification of co-expressed gene modules in excitatory neurons
gene module
number of genes
increased in stimulation
decreased in stimulation
Ex–7 61
Ex–6 29
Ex–5 58
Ex–4 36
Ex–3 114
Ex–2 170
Ex–1 343
Signed –log10(p value)
F
Ex–3
Ex–6
Ex–7
G
Ex-3
regulation of synapse organization
neurotransmitter receptor activity
regulation of presynapse assembly
axon extension
-log10 (p value)
Ex-6
regulation of membrane potential
phosphatidylinositol 3-kinase signaling
-log10 (p value)
Ex-7
neuron projection development
adherens junction organization
trans-synaptic signaling
-log10 (p value)
H
flickering light & sound at 40 Hz (stimulation)
ambient light & sound (ambient)
Days of experiment
perfusion after the experiment and IHC for PSD95 and Synaptophysin
Quantification of colocalized signals
ambient
stimulation
Synaptophysin
PSD95
DAPI
ambient
stimulation
Synaptophysin-PSD95 colocalized puncta (relative to ambient)
I
Hub genes overlapped with AD associated genes
Reln
Efna5
Adra1a
Adcy8
Pcdh11x
Lrrc4c
Cobl
Gpc6
Gap43
Farp1
Vsnl1
Gira4
J
DAPI
Reelin
NeuN
merged
ambient
stimulation
ambient
stimulation
% Reln+ neurons
K
Aging
Ex–3
Ex–6
Ex–7
Fold enrichment
bulk RNAseq, old
Ex Neurons, old
Ex Neurons, old
vs young subjects
L
Alzhiemer's Disease (AD)
Ex–3
Ex–6
Ex–7
Fold enrichment
bulk RNAseq, 4 months, AD
bulk RNAseq, 8 months, AD
Ex Neurons, AD
Ex Neurons, patients with AD
vs healthy subjects

Fig 3

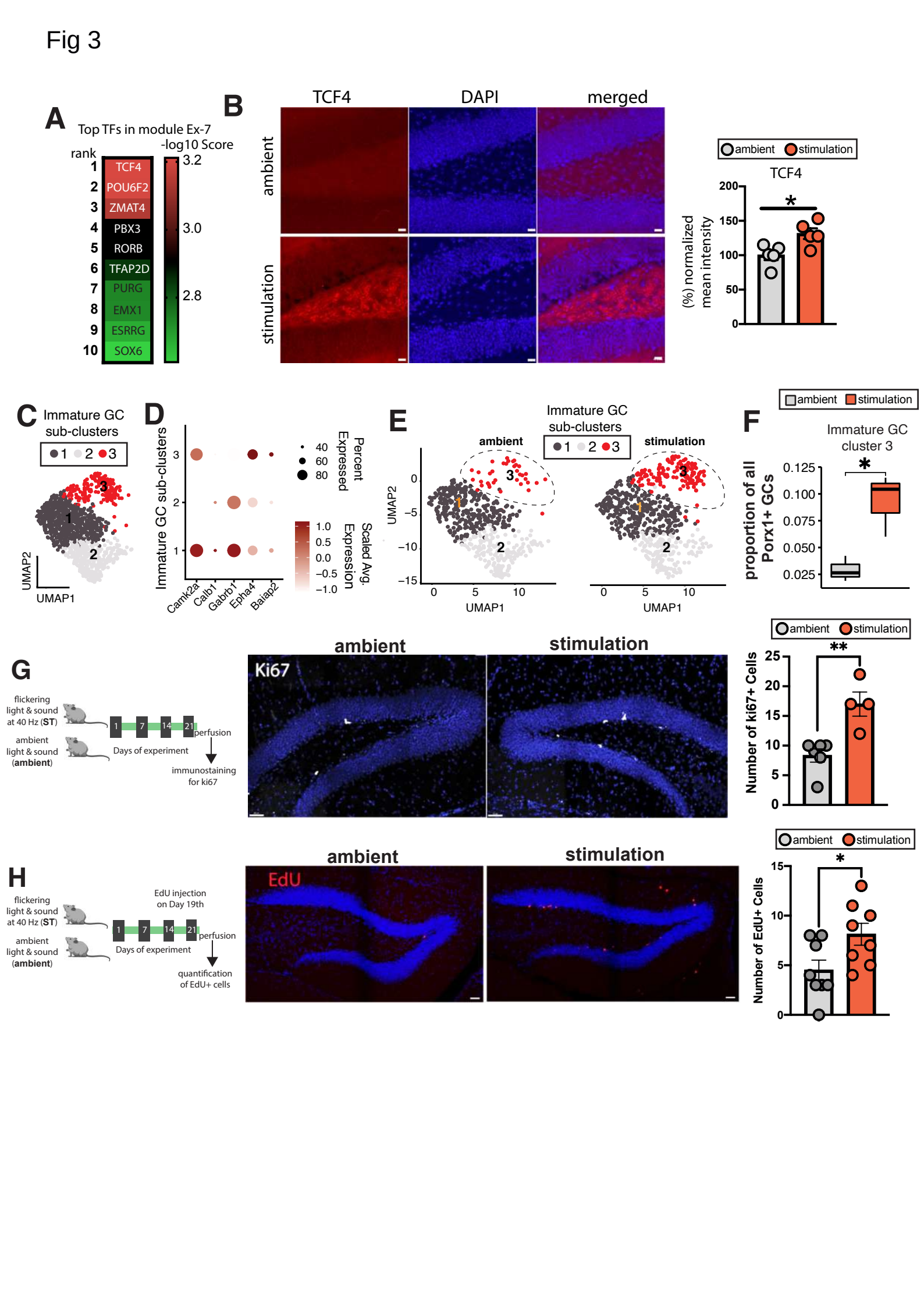
A
Top TFs in module Ex-7
-log10 Score
rank
1 TCF4
2 POU6F2
3 ZMAT4
4 PBX3
5 RORB
6 TFAP2D
7 PURG
8 EMX1
9 ESRRG
10 SOX6
3.2
3.0
2.8
B
TCF4
DAPI
merged
ambient
stimulation
ambient
stimulation
TCF4
(%) normalized mean intensity
200
150
100
50
0
*
C
Immature GC sub-clusters
1 2 3
UMAP2
UMAP1
D
Immature GC sub-clusters
Camk2a
Calb1
Gabrb1
Epha4
Baiap2
Percent Expressed
40
60
80
Scaled Avg. Expression
1.0
0.5
0.0
−0.5
−1.0
E
Immature GC sub-clusters
ambient
stimulation
1 2 3
UMAP2
UMAP1
F
ambient
stimulation
Immature GC cluster 3
proportion of all Porx1+ GCs
0.125
0.100
0.075
0.050
0.025
*
G
flickering light & sound at 40 Hz (ST)
ambient light & sound (ambient)
1
7
14
21
perfusion
Days of experiment
immunostaining for ki67
ambient
stimulation
Ki67
ambient
stimulation
Number of ki67+ Cells
25
20
15
10
5
0
**
H
flickering light & sound at 40 Hz (ST)
ambient light & sound (ambient)
EdU injection on Day 19th
1
7
14
21
perfusion
Days of experiment
quantification of EdU+ cells
ambient
stimulation
EdU
ambient
stimulation
Number of EdU+ Cells
15
10
5
0
*

Fig S1

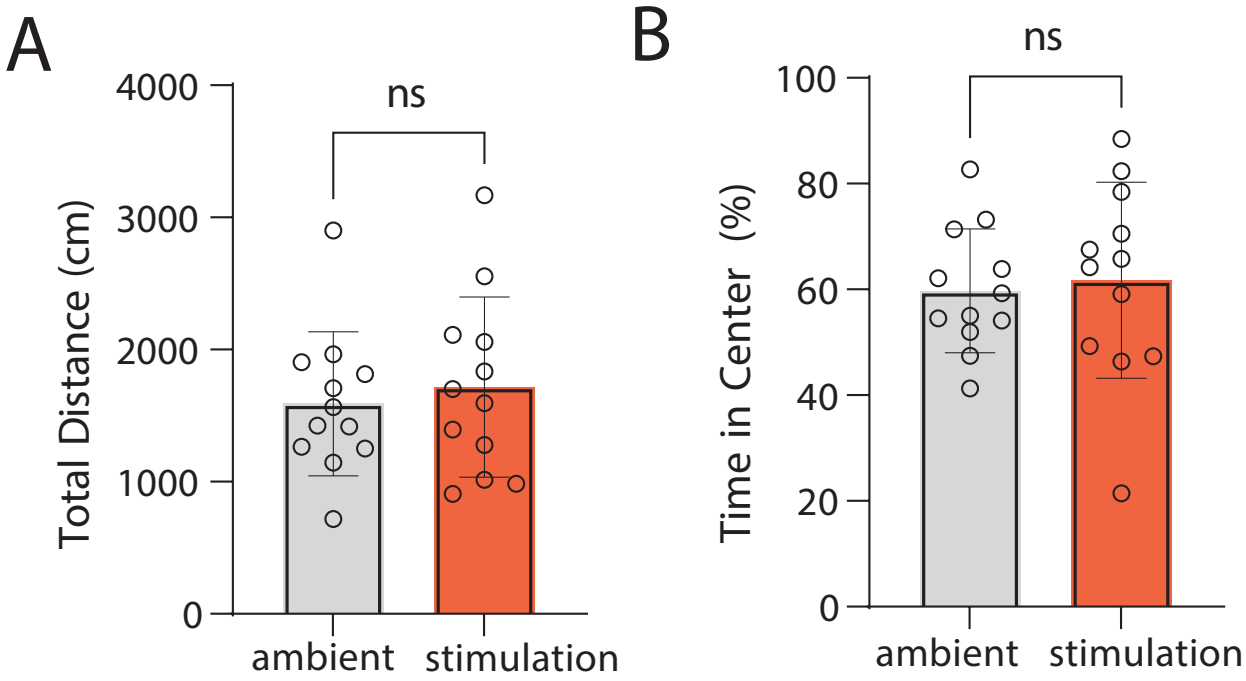
A
4000
3000
2000
1000
0
Total Distance (cm)
ns
ambient
stimulation
B
100
80
60
40
20
0
Time in Center (%)
ns
ambient
stimulation

Fig S2

A
flickering
light & sound
at 40 Hz (stimulation)
ambient
light & sound
(ambient)
1
7
14
21
Days of experiment
perfusion
immunostaining

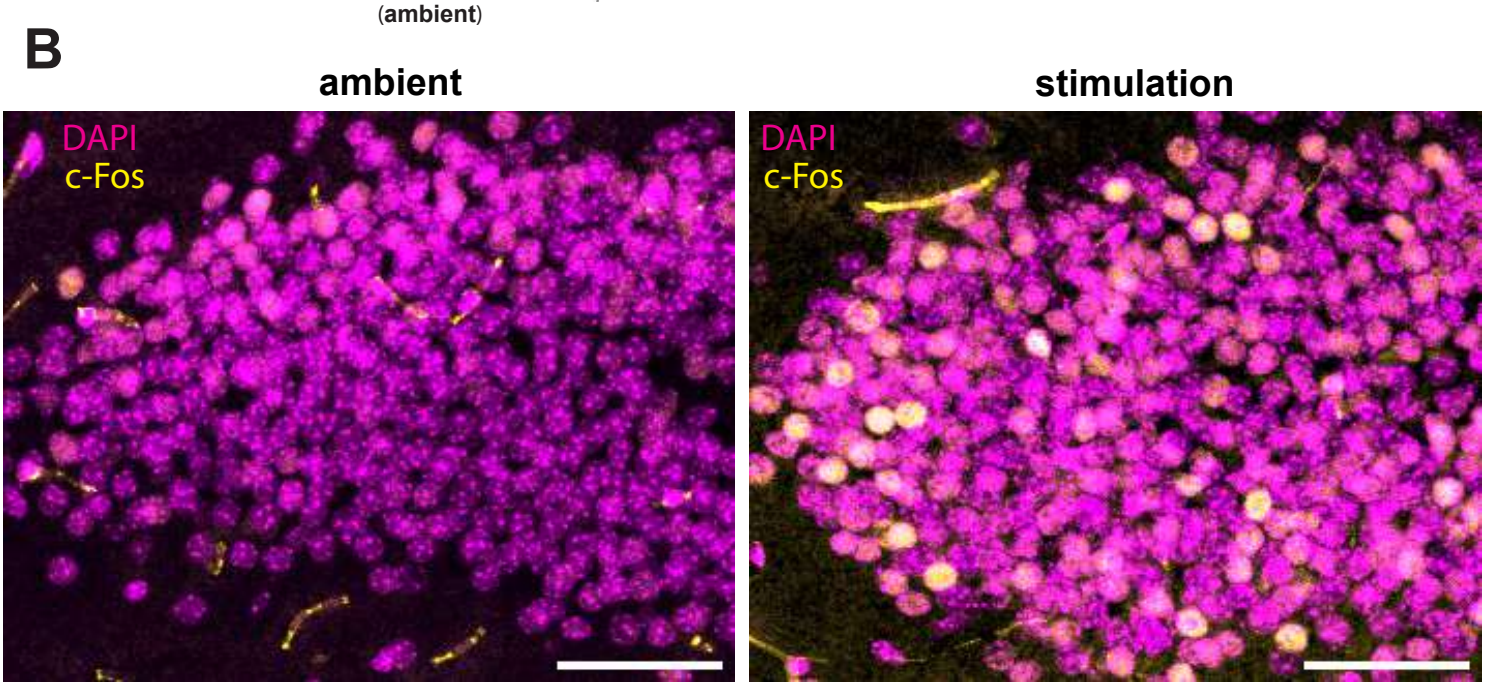
B
ambient
stimulation
DAPI
c-Fos
DAPI
c-Fos

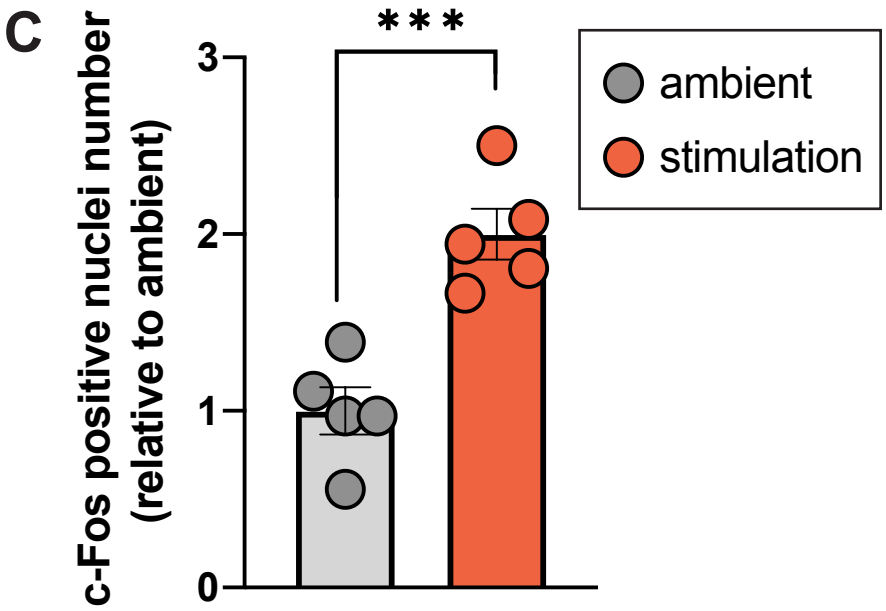
C
c-Fos positive nuclei number
(relative to ambient)
0
1
2
3
***
ambient
stimulation

Fig S3

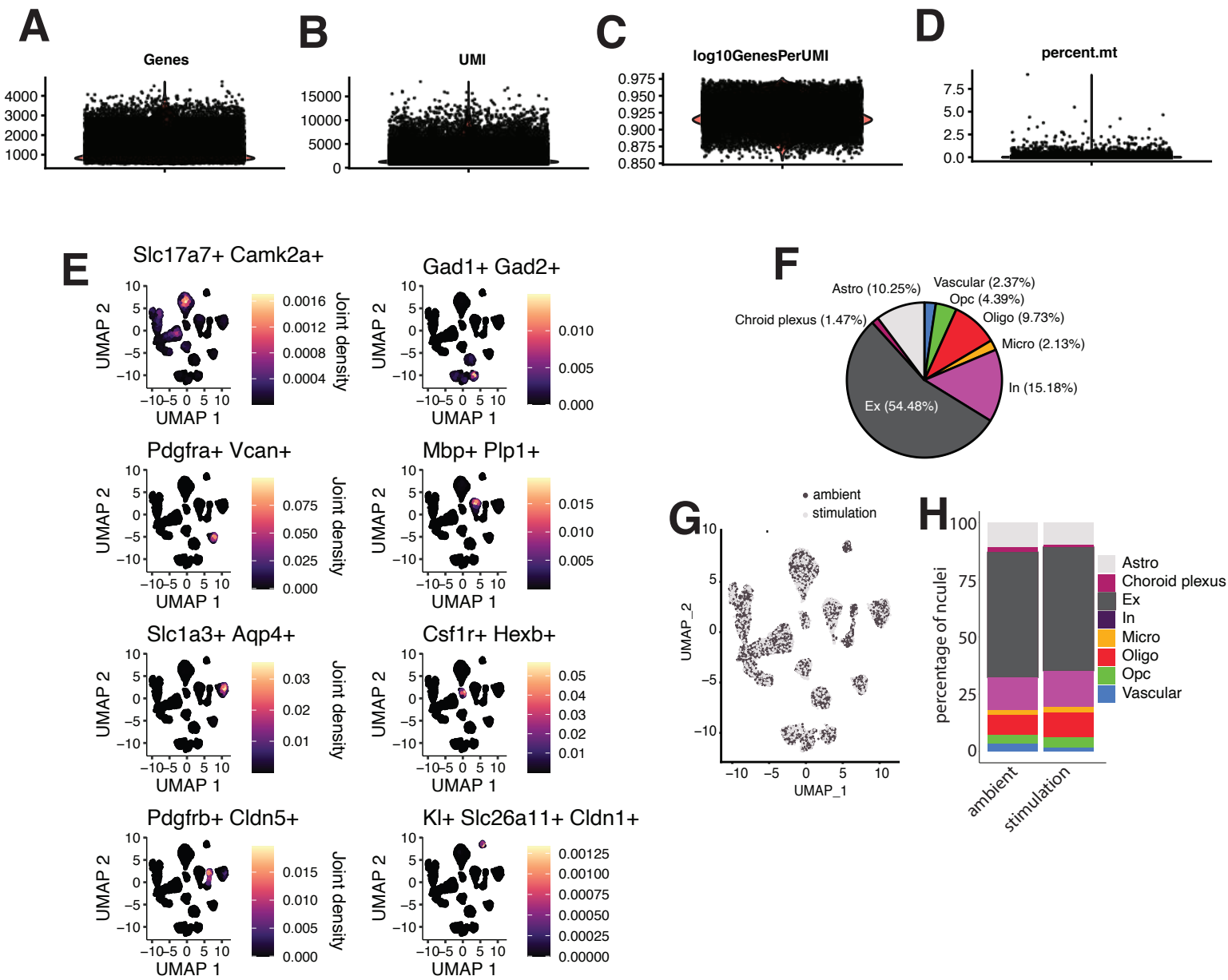
A
Genes
B
UMI
C
log10GenesPerUMI
D
percent.mt
E
Slc17a7+ Camk2a+
Gad1+ Gad2+
Pdgfra+ Vcan+
Mbp+ Plp1+
Slc1a3+ Aqp4+
Csf1r+ Hexb+
Pdgfrb+ Cldn5+
Kl+ Slc26a11+ Cldn1+
UMAP 1
UMAP 2
Joint density
F
Astro (10.25%)
Vascular (2.37%)
Opc (4.39%)
Oligo (9.73%)
Micro (2.13%)
In (15.18%)
Ex (54.48%)
Chroid plexus (1.47%)
G
ambient
stimulation
UMAP_1
UMAP_2
H
percentage of nculei
ambient
stimulation
Astro
Choroid plexus
Ex
In
Micro
Oligo
Opc
Vascular

Fig S4

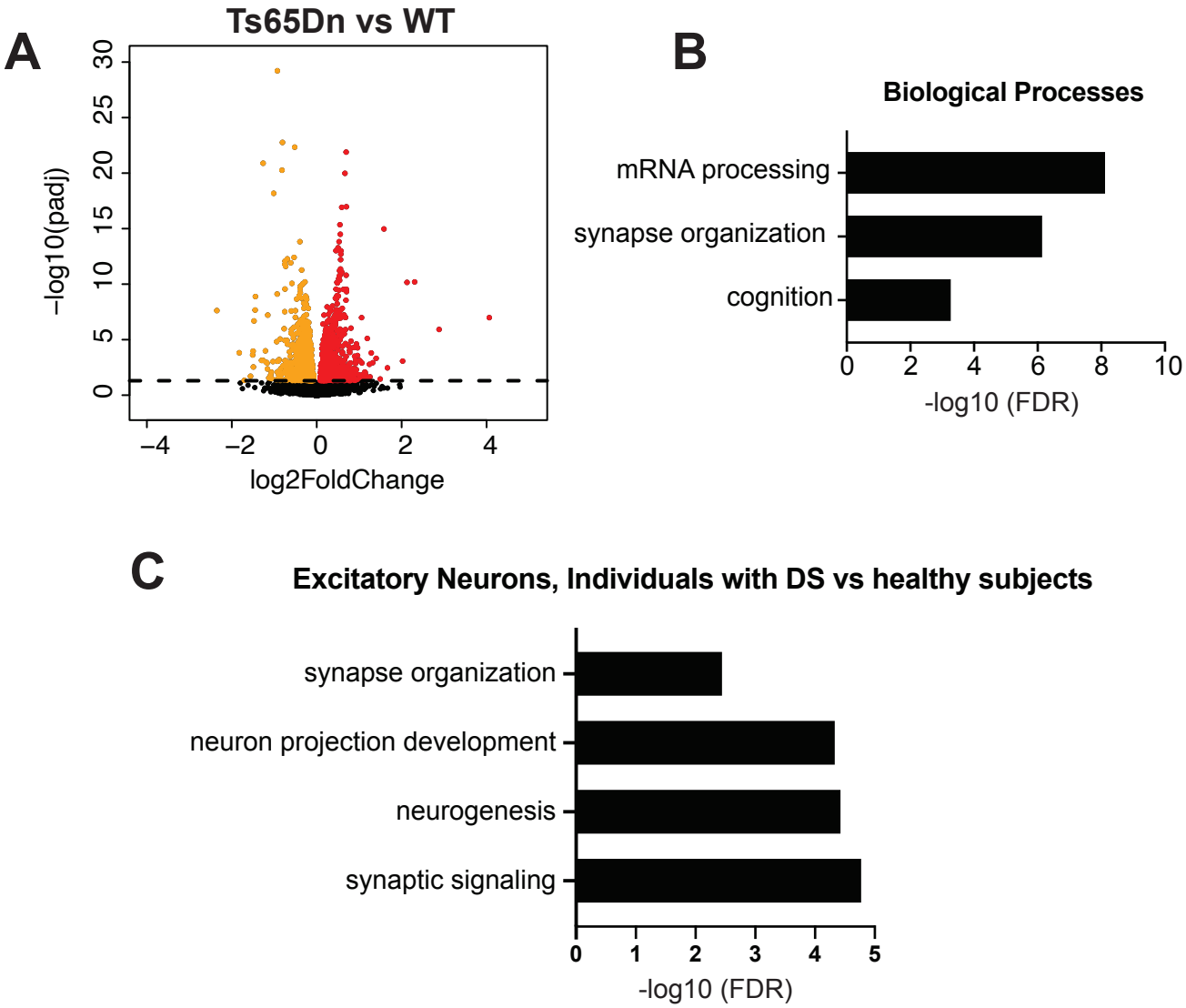
A
Ts65Dn vs WT
−log10(padj)
0
5
10
15
20
25
30
−4
−2
0
2
4
log2FoldChange
B
Biological Processes
mRNA processing
synapse organization
cognition
0
2
4
6
8
10
-log10 (FDR)
C
Excitatory Neurons, Individuals with DS vs healthy subjects
synapse organization
neuron projection development
neurogenesis
synaptic signaling
0
1
2
3
4
5
-log10 (FDR)

Fig S5

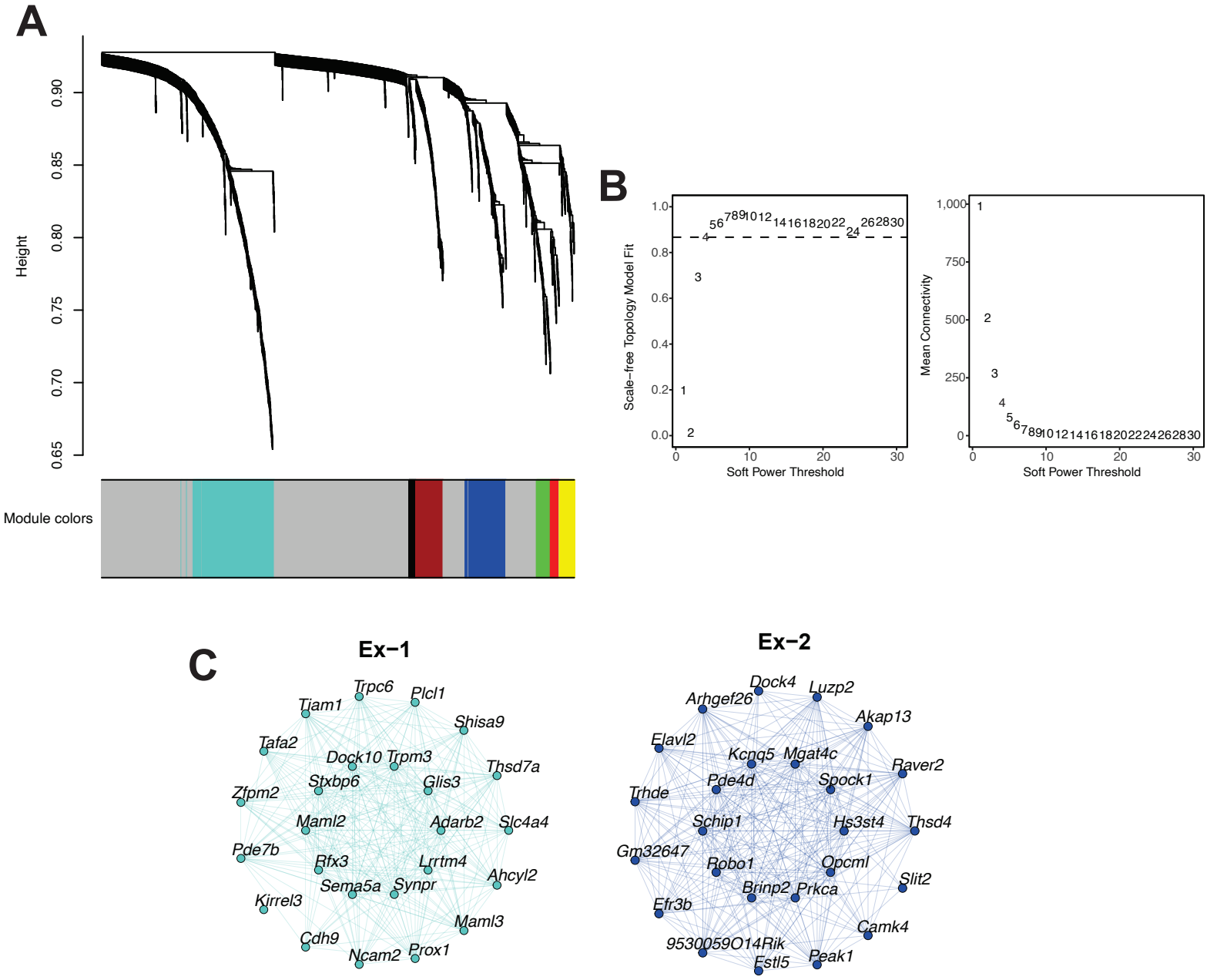
A
Height
0.65
0.70
0.75
0.80
0.85
0.90
Module colors
B
Scale−free Topology Model Fit
Soft Power Threshold
Mean Connectivity
Soft Power Threshold
C
Ex−1
Trpc6
Plcl1
Tiam1
Shisa9
Tafa2
Dock10
Trpm3
Thsd7a
Stxbp6
Glis3
Zfpm2
Maml2
Adarb2
Slc4a4
Pde7b
Rfx3
Lrrtm4
Ahcyl2
Sema5a
Synpr
Kirrel3
Maml3
Cdh9
Ncam2
Prox1
Ex−2
Dock4
Luzp2
Arhgef26
Akap13
Elavl2
Kcnq5
Mgat4c
Raver2
Pde4d
Spock1
Trhde
Schip1
Hs3st4
Thsd4
Gm32647
Robo1
Opcml
Slit2
Brinp2
Prkca
Efr3b
Camk4
9530059O14Rik
Peak1
Fstl5

Fig S6

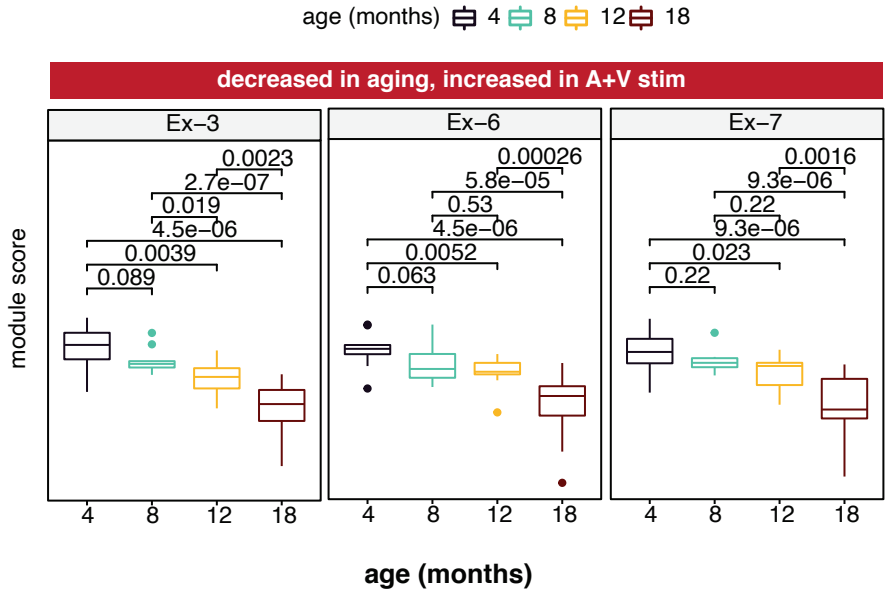
age (months) 4 8 12 18
decreased in aging, increased in A+V stim
Ex−3
Ex−6
Ex−7
module score
0.0023
2.7e−07
0.019
4.5e−06
0.0039
0.089
0.00026
5.8e−05
0.53
4.5e−06
0.0052
0.063
0.0016
9.3e−06
0.22
9.3e−06
0.023
0.22
4
8
12
18
age (months)

Fig S7

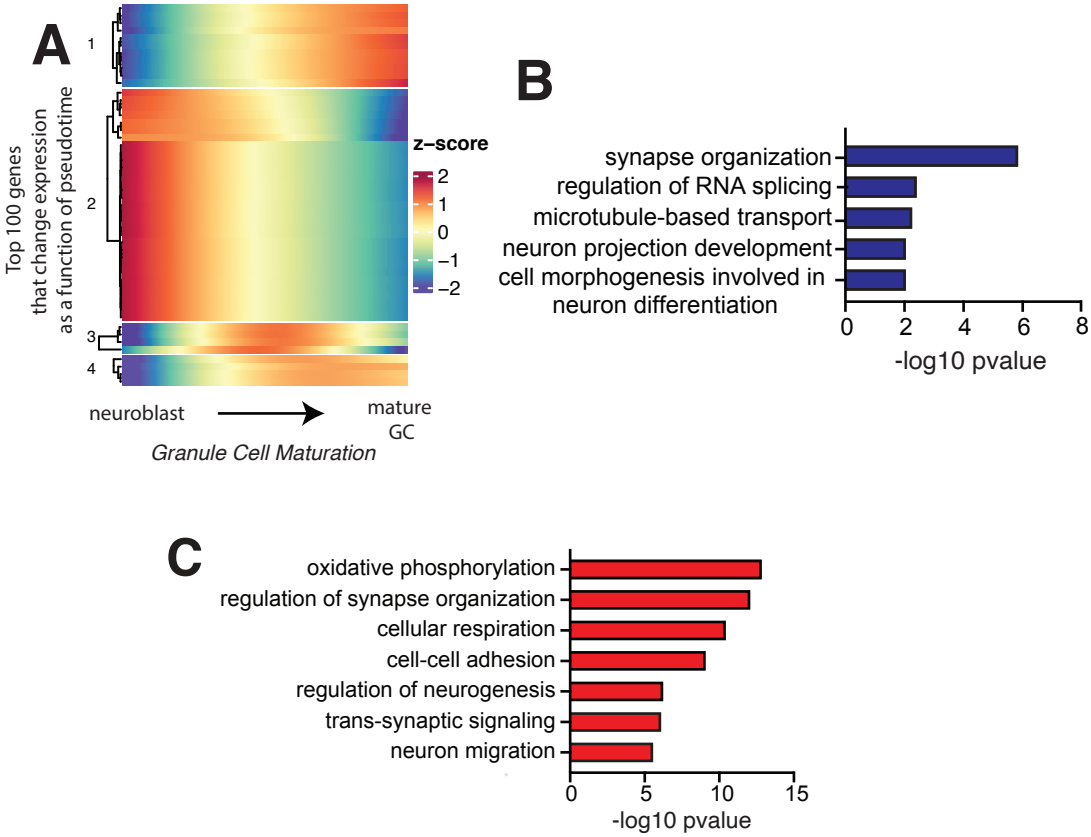
A
Top 100 genes
that change expression
as a function of pseudotime
1
2
3
4
z–score
2
1
0
−1
−2
neuroblast
mature
GC
Granule Cell Maturation
B
synapse organization
regulation of RNA splicing
microtubule-based transport
neuron projection development
cell morphogenesis involved in
neuron differentiation
0
2
4
6
8
-log10 pvalue
C
oxidative phosphorylation
regulation of synapse organization
cellular respiration
cell-cell adhesion
regulation of neurogenesis
trans-synaptic signaling
neuron migration
0
5
10
15
-log10 pvalue